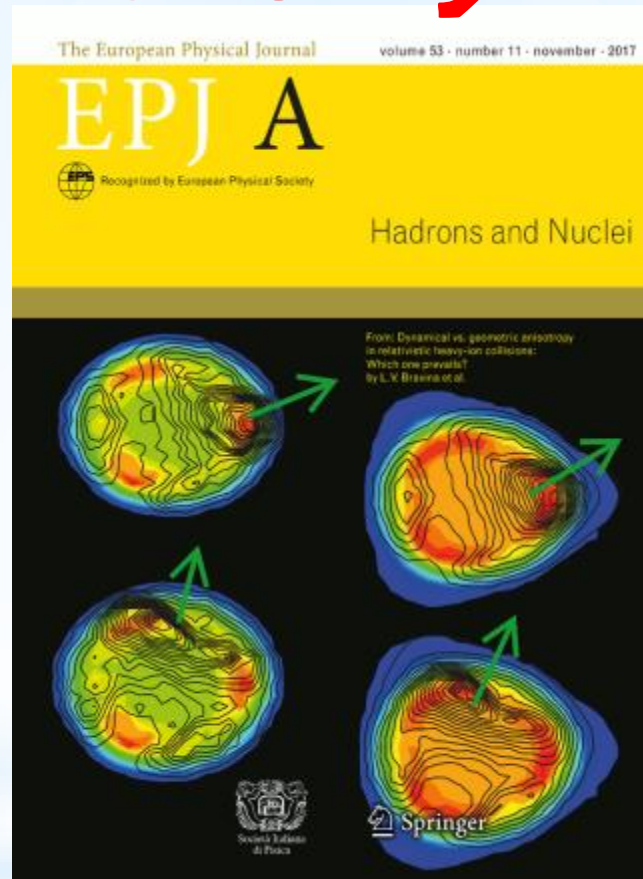


Dynamical vs geometric anisotropy in relativistic heavy-ion collisions



L.Bravina, E. Zabrodin,
in collaboration with

I. Lokhtin, L. Malinina, S. Petrushanko and A. Snigirev

25th Nordic Particle Physics Meeting, Spåtind , Norway, January 2–7, 2018

Outline

- I. HYDroynamics with JETs (HYDJET++) model
- II. Description of elliptic and triangular flow in relativistic heavy-ion collisions
- III. Femtoscopic correlations
- IV. Geometric and dynamical anisotropy
- V. Flow and oscillations of the femtoscopic radii (simultaneous description)
- VI. Conclusions

An aerial photograph of a river with white water rapids. The water is a vibrant turquoise color, and the rapids are a frothy white. The text is overlaid in the center of the image.

**I. HYDJET++ =
FASTMC + HYDJET**

Dynamic Regimes

Parton distribution,
Nuclear geometry
Nuclear shadowing

Parton production &
regeneration
(or, sQGP)

Chemical freeze-out
(Quark recombination)

Jet fragmentation
functions

Hadron rescattering

Thermal freeze-out

Hadron decays

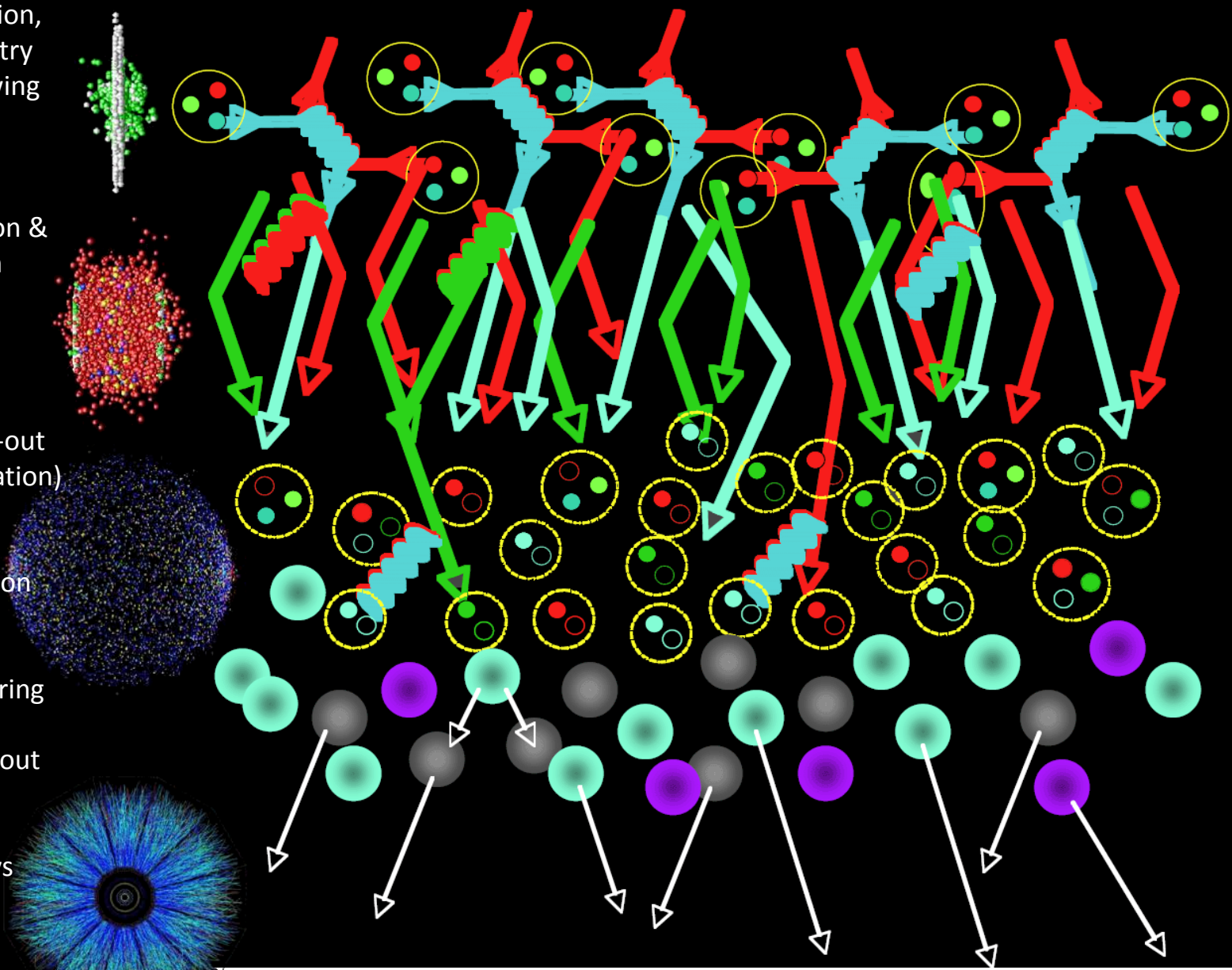
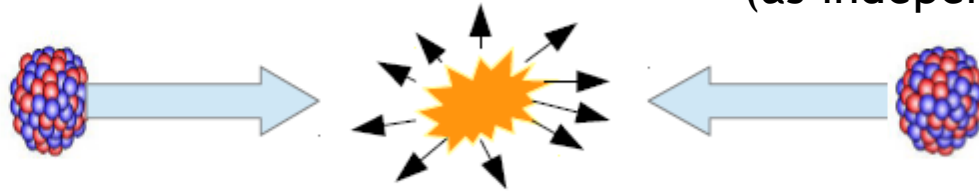


Diagram by Peter Steinberg

HYDJET++ model for heavy ion collisions

Simplifies the pictures of heavy ion collisions as merging of 2 components:
(as independent parts)



➤ **soft hydro-type part**
(represented by hadron emission
assuming thermal equilibrium)

Based on the adapted FAST MC model:

N.S.Amelin, R.Lednisky, T.A.Pocheptsov, I.P.Lokhtin,
L.V.Malinina, A.M.Snigirev, Yu.A.Karpenko,
Yu.M.Sinyukov, *Phys. Rev. C* 74 (2006) 064901

N.S.Amelin, R.Lednisky, I.P.Lokhtin, L.V.Malinina,
A.M.Snigirev, Yu.A.Karpenko, Yu.M.Sinyukov,
I.C.Arsene, L.Bravina, *Phys. Rev. C* 77 (2008) 014903

HYDJET++ (soft): main physics assumptions

A hydrodynamic expansion of the fireball is supposed to **end by a sudden system breakup** at given T and chemical potentials. Momentum distribution of produced hadrons keeps the thermal character of the equilibrium distribution.

Cooper-Frye formula:

$$p^0 \frac{d^3 N_i}{d^3 p} = \int_{\sigma(x)} d^3 \sigma_\mu(x) p^\mu f_i^{eq}(p^\nu u_\mu(x); T, \mu_i)$$

- HYDJET++ avoids straightforward 6-dimensional integration by using the special simulation procedure (like HYDJET): momentum generation in the rest frame of fluid element, then Lorentz transformation in the global frame \rightarrow uniform weights \rightarrow effective von-Neumann rejection-acceptance procedure.

Freeze-out surface parameterizations

1. The Bjorken model with hypersurface

$$\tau = (t^2 - z^2)^{1/2} = \text{const}$$

2. Linear transverse flow rapidity profile

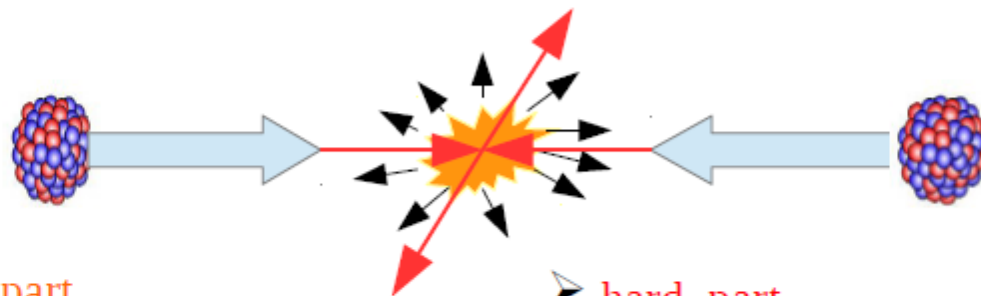
$$\rho_u = \frac{r}{R} \rho_u^{\max}$$

3. The total effective volume for particle production at

$$- V_{\text{eff}} = \int_{\sigma(x)} d^3 \sigma_\mu(x) u^\mu(x) = \tau \int_0^R \gamma_r r dr \int_0^{2\pi} d\phi \int_{\eta_{\min}}^{\eta_{\max}} d\eta = 2\pi\tau\Delta\eta \left(\frac{R}{\rho_u^{\max}} \right)^2 (\rho_u^{\max} \sinh \rho_u^{\max} - \cosh \rho_u^{\max} + 1)$$

HYDJET++ model for heavy ion collisions

Simplifies the pictures of heavy ion collisions as merging of 2 components:



➤ **soft hydro-type part**
(represented by hadron emission
assuming thermal equilibrium)

➤ **hard part**
(represented by hard parton scattering and
later hadronization)

Based on PYTHIA with quenching:
PYQUEN: I.P.Lokhtin, A.M.Snigirev,
Eur. Phys. J. 45 (2006) 211

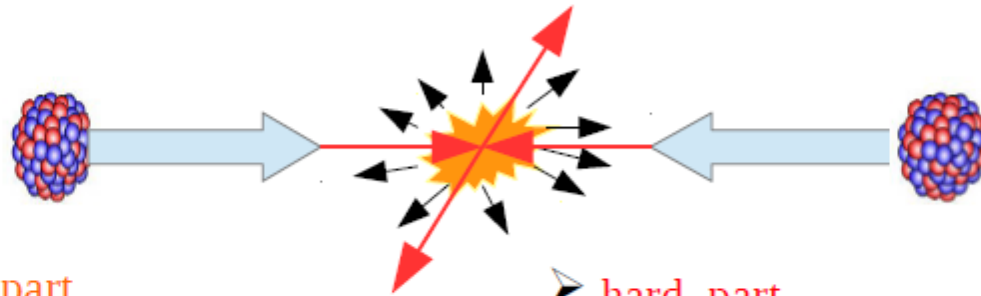
Nuclear shadowing is accounted for:
K.Tywoniuk et al., Phys. Lett. B 657 (2007) 170

<http://cern.ch/lokhtin/hydjet++>
(latest version 2.3)

I.Lokhtin, L.Malinina, S.Petrushanko, A.Snigirev, I.Arsene, K.Tywoniuk,
Comp.Phys.Comm. 180 (2009) 779

HYDJET++ model for heavy ion collisions

Simplifies the pictures of heavy ion collisions as merging of 2 components:

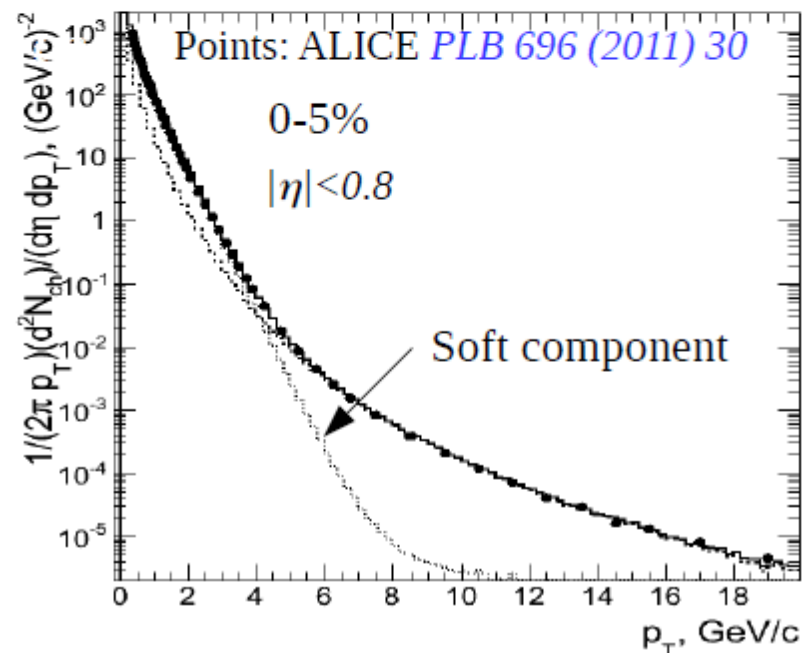


➤ **soft hydro-type part**
(represented by hadron emission assuming thermal equilibrium)

➤ **hard part**
(represented by hard parton scattering and later hadronization based on PYTHIA)

Soft and hard components:

- The contribution of the hard part to the total multiplicity is control by p_{Tmin} parameter (parton hard scattering in PYTHIA)
- Modification of the hard part due to interactions with the medium is simulated
- No modification of soft part



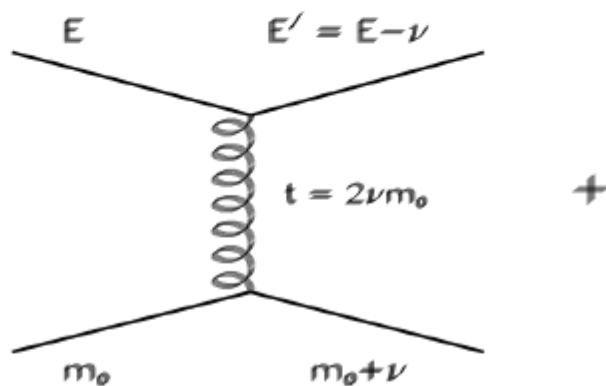
Hard component



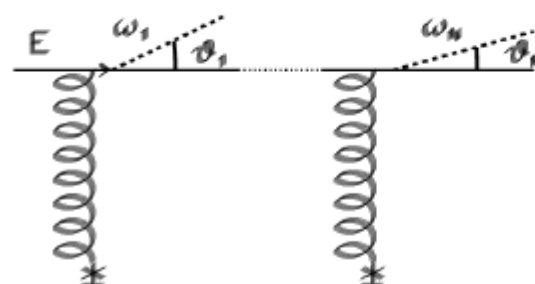
Energy loss, general kinetic integral equation with scattering probability density:

$$\Delta E(L, E) = \int_0^L dl \frac{dP(l)}{dl} \lambda(l) \frac{dE(l, E)}{dl} \quad \frac{dP(l)}{dl} = \frac{1}{\lambda(l)} \exp(-l/\lambda(l))$$

- Collisional loss
(high momentum transfer approximation)



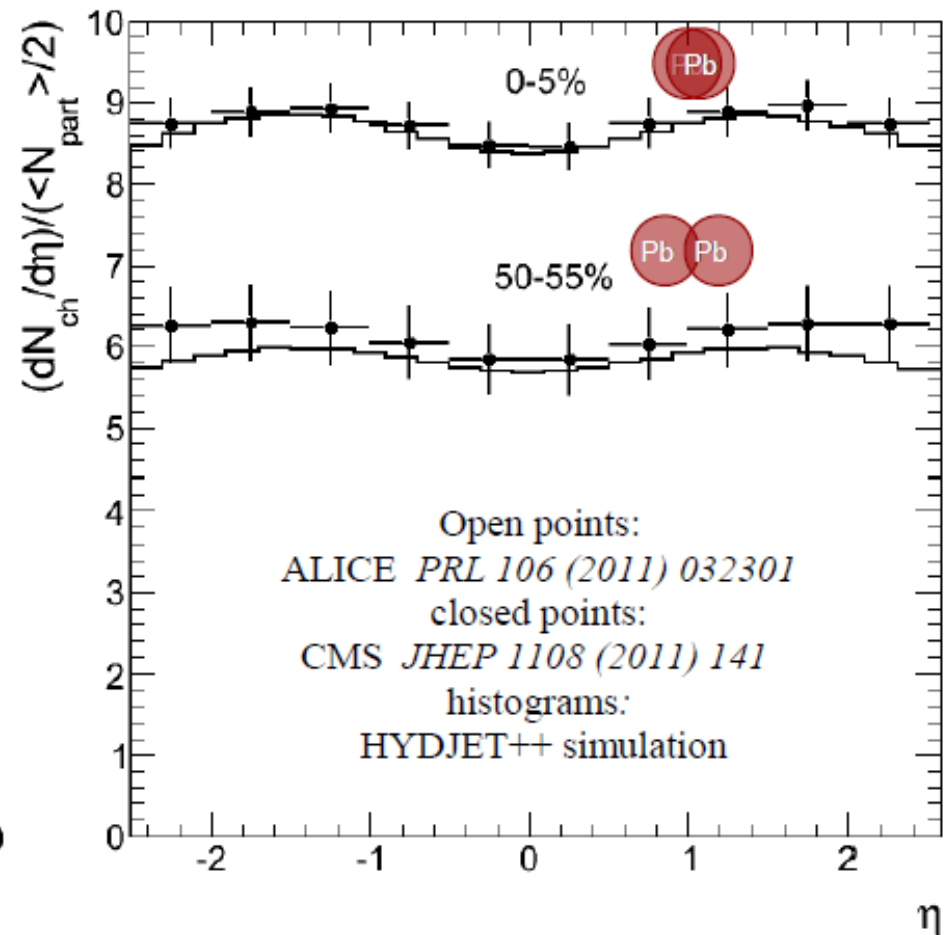
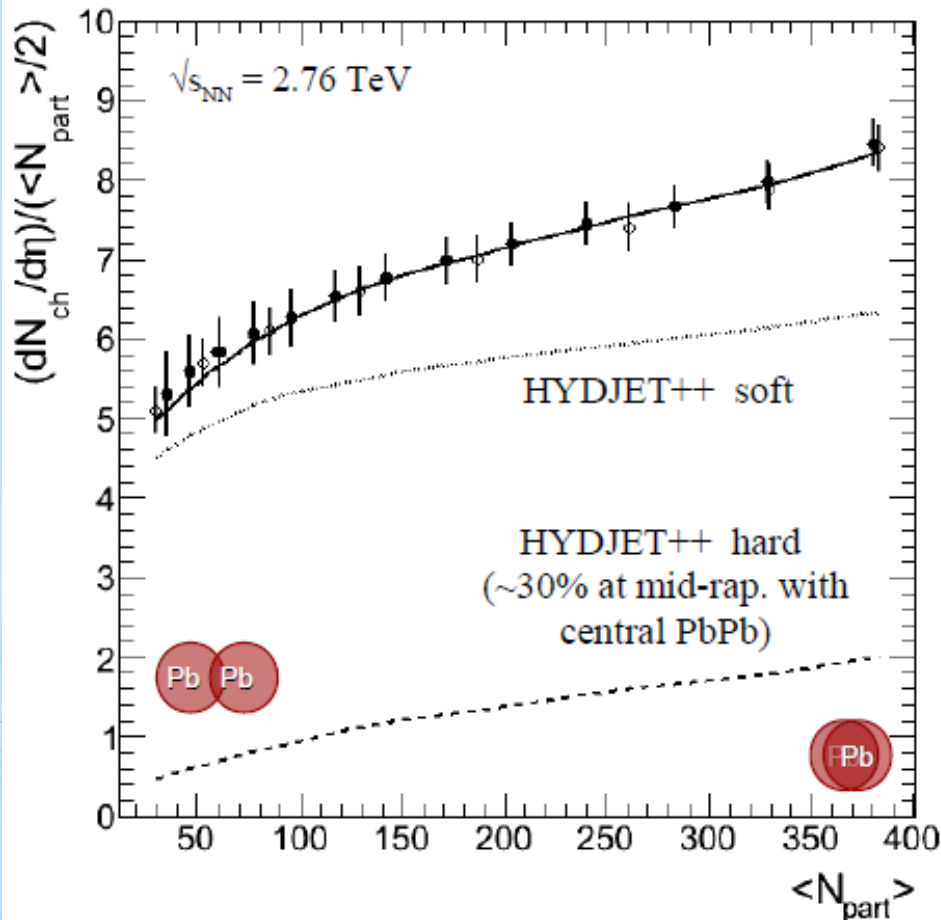
- Radiative loss (coherent gluon radiation in Baier-Dokshitzer-Mueller-Schiff formalism)



- “Dead” cone approximation for massive quarks

Charged multiplicity vs centrality and pseudorapidity in HYDJET++ at LHC

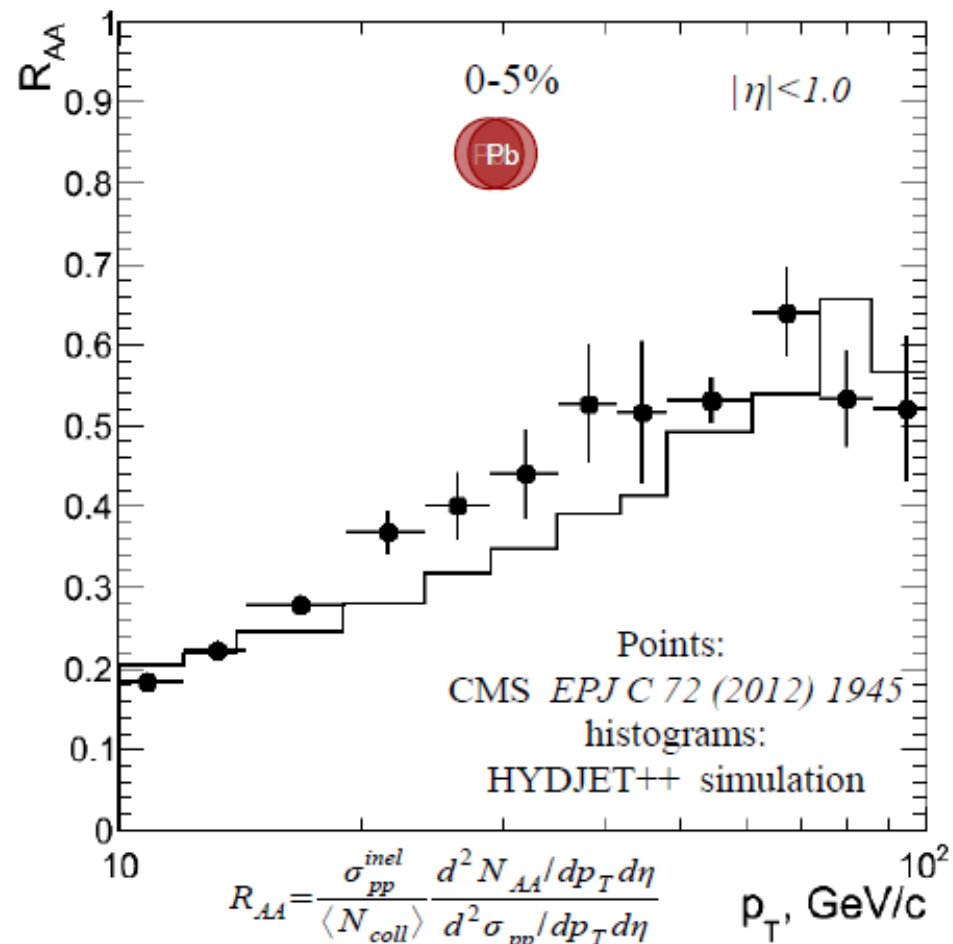
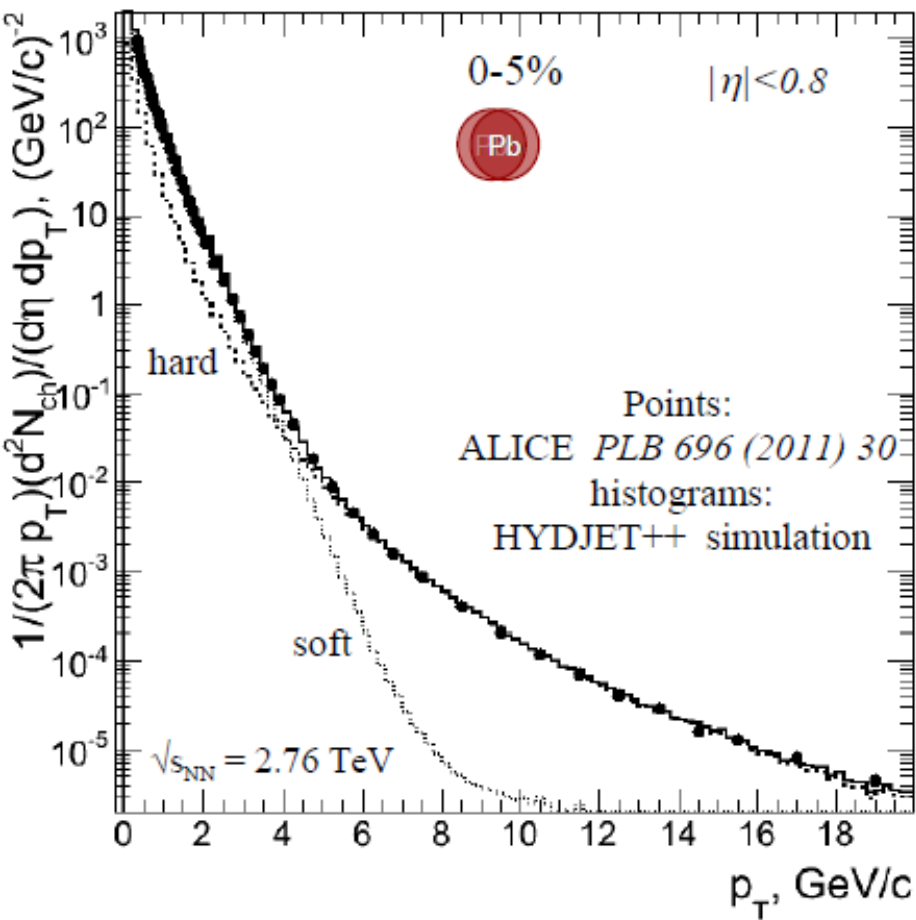
I.P. Lokhtin, A.V. Belyaev, L.V. Malinina, S.V. Petrushanko, E.P. Rogochaya, A.M. Snigirev, Eur.Phys.J. C (2012) 72:2045



Tuned HYDJET++ reproduces multiplicity vs. event centrality down to very peripheral events, as well as approximately flat pseudorapidity distribution.

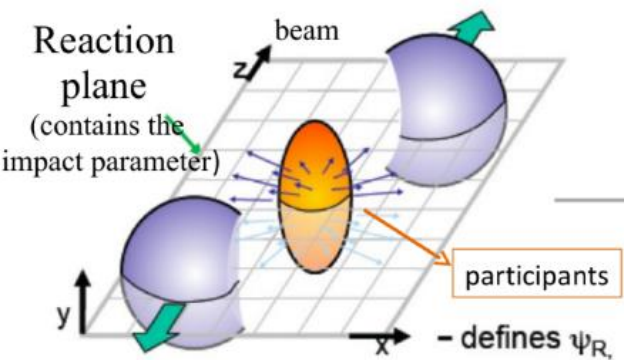
P_T spectrum and R_{AA} factor for charged hadrons in HYDJET++ at LHC

I.P. Lokhtin, A.V. Belyaev, L.V. Malinina, S.V. Petrushanko, E.P. Rogochaya, A.M. Snigirev, *Eur.Phys.J. C* (2012) 72:2045



HYDJET++ reproduces p_T -spectrum and R_{AA} for central PbPb collisions in mid-rapidity up to $p_T \sim 100 \text{ GeV/c}$.

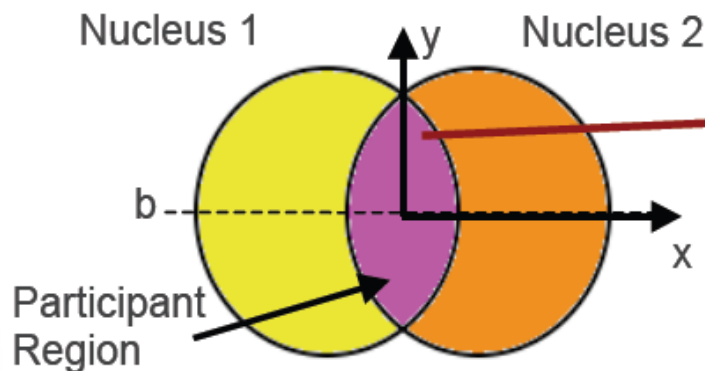
**II. Elliptic and Triangular
flow in HYDJET++ :
interplay
of hydrodynamics and jets**



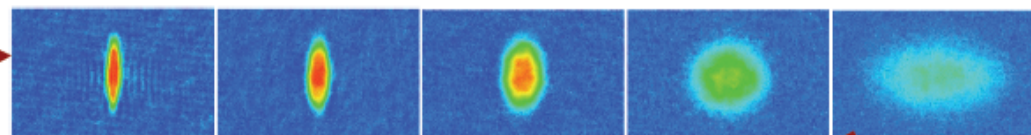
ELLIPTIC FLOW

Initial spatial anisotropy is converted to anisotropy in momentum space

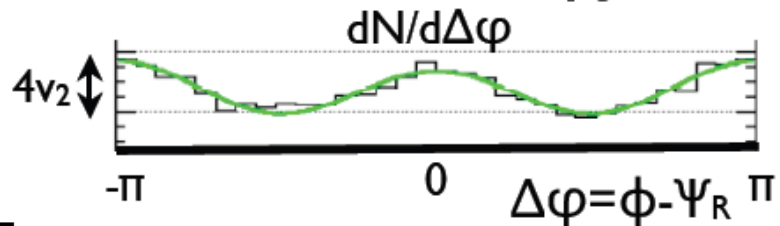
Initial anisotropy



Pressure driven expansion



Final anisotropy



$$\frac{dN}{d\phi} = \frac{N}{2\pi} \left(1 + \sum 2v_n \cos(n(\phi - \psi_R)) \right)$$

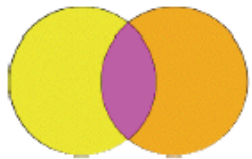
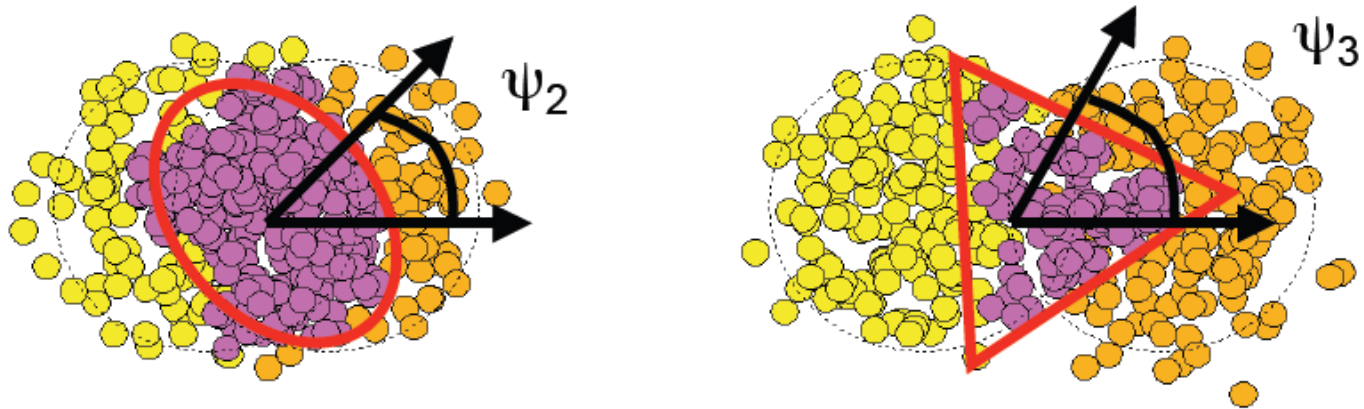
S.Voloshin, Y.Zhang, Z.Phys.C70 (1996) 665

$$v_2 = \langle \cos(2(\phi - \psi_R)) \rangle \propto \varepsilon$$

Elliptic flow is quantified by the second Fourier coefficient (v_2) of the observed particle distribution

TRIANGULAR FLOW

B. Alver and G.Roland, PRC 81 (2010) 054905



$$\frac{dN}{d\phi} = \frac{N}{2\pi} \left(1 + \sum 2v_n \cos(n(\phi - \psi_R)) \right)$$

$$v_2 = \langle \cos(2(\phi - \psi_R)) \rangle$$

$$v_3 = 0$$



$$\frac{dN}{d\phi} = \frac{N}{2\pi} \left(1 + \sum 2v_n \cos(n(\phi - \psi_n)) \right)$$

$$v_2 = \langle \cos(2(\phi - \psi_2)) \rangle$$

$$v_3 = \langle \cos(3(\phi - \psi_3)) \rangle$$

The triangular initial shape leads to triangular hydrodynamic flow

Anisotropic flow generation in HYDJET++

Elliptic flow v_2

$$v_2 \propto \frac{2(\delta - \epsilon)}{(1 - \delta^2)(1 - \epsilon^2)}$$

- ✓ Spatial modulation of freeze-out surface;
- ✓ fluid velocity modulation.

Spatial anisotropy

Momentum anisotropy

$$\epsilon(b) = \frac{R_y^2 - R_x^2}{R_y^2 + R_x^2}$$

$$\tan \varphi_u = \sqrt{\frac{1 - \delta(b)}{1 + \delta(b)}} \tan \varphi$$

$R(b)$ – surface radius φ_u – azimuthal angle of fluid velocity
 φ – spatial azimuthal angle

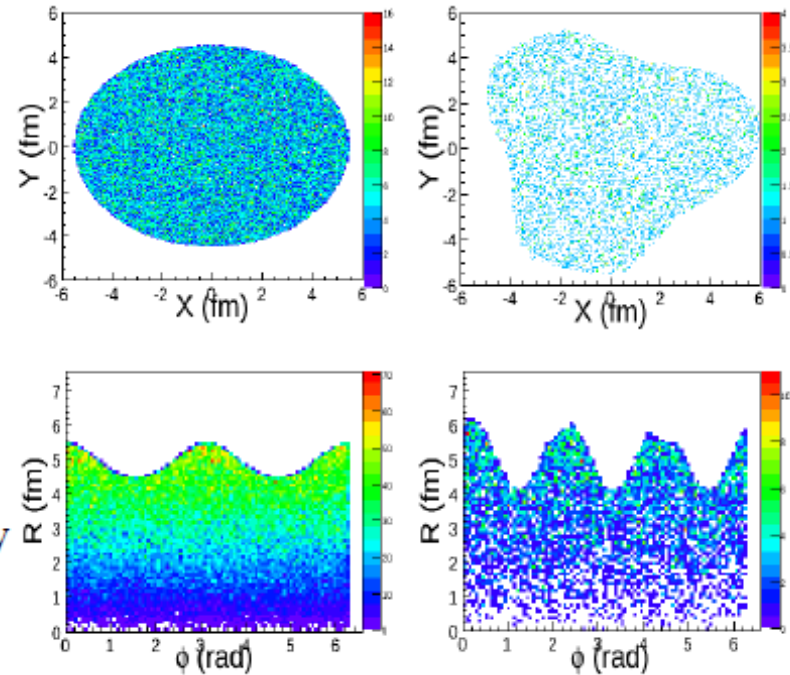
Triangular flow v_3

Spatial anisotropy

$$R(b, \phi) = R_{\text{ell}}(b, \phi) \{1 + \epsilon_3(b) \cos [3(\phi - \Psi_3)]\}, \quad R_{\text{ell}}(b, \phi) = R_{\text{fo}}(b) \frac{\sqrt{1 - \epsilon^2(b)}}{\sqrt{1 + \epsilon(b) \cos 2\phi}}$$

Momentum anisotropy

$$\rho_u^{\text{max}}(b) = \rho_u^{\text{max}}(0) \{1 + \rho_3(b) \cos [3(\phi - \Psi_{EP,3})] + \dots\}$$

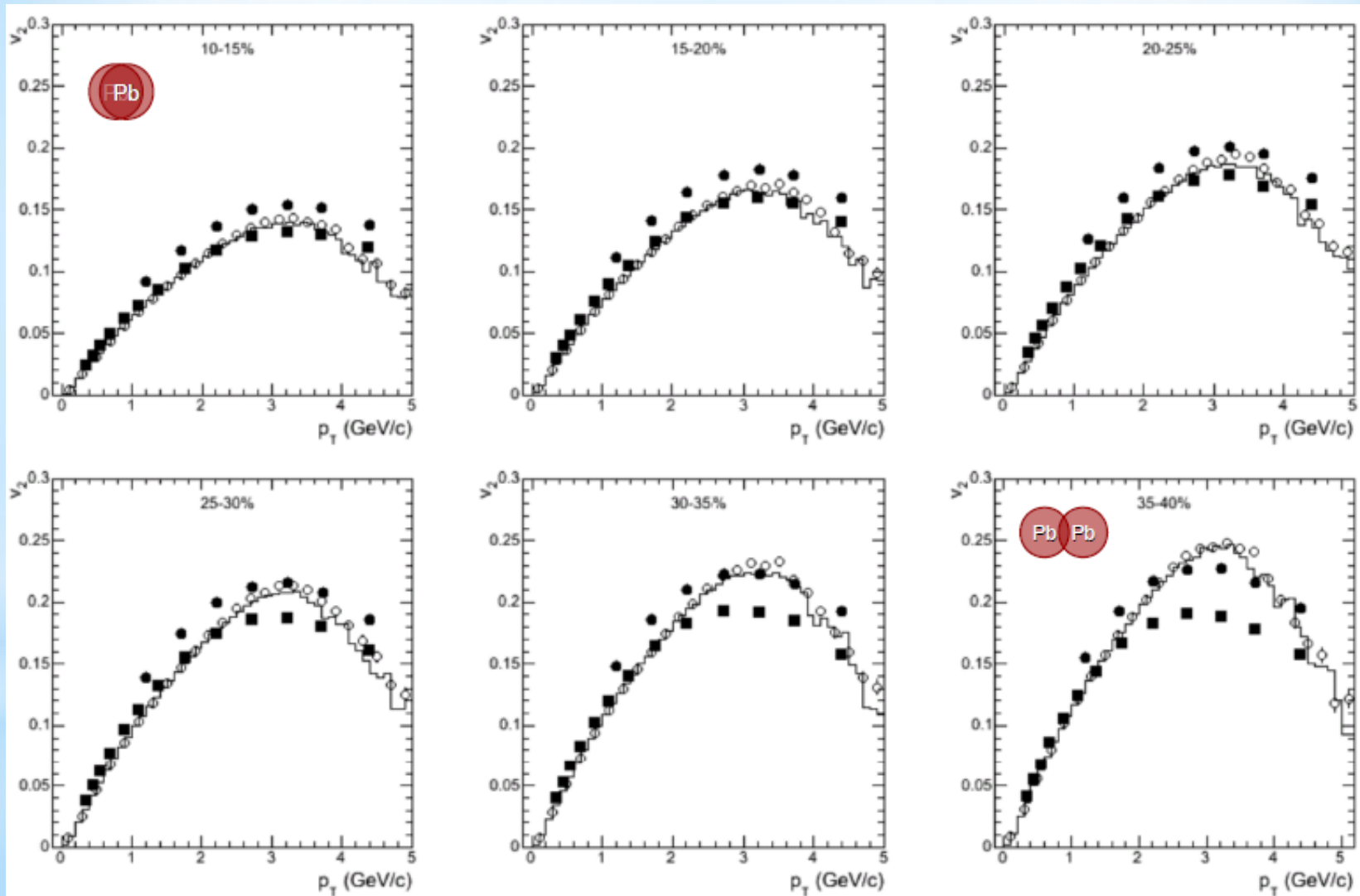


Four parameters ϵ , ϵ_3 , δ , ρ_3 are tuned to fit experimental data

LHC data vs. HYDJET++ model

Elliptic flow

Pb+Pb @ 2.76 ATeV



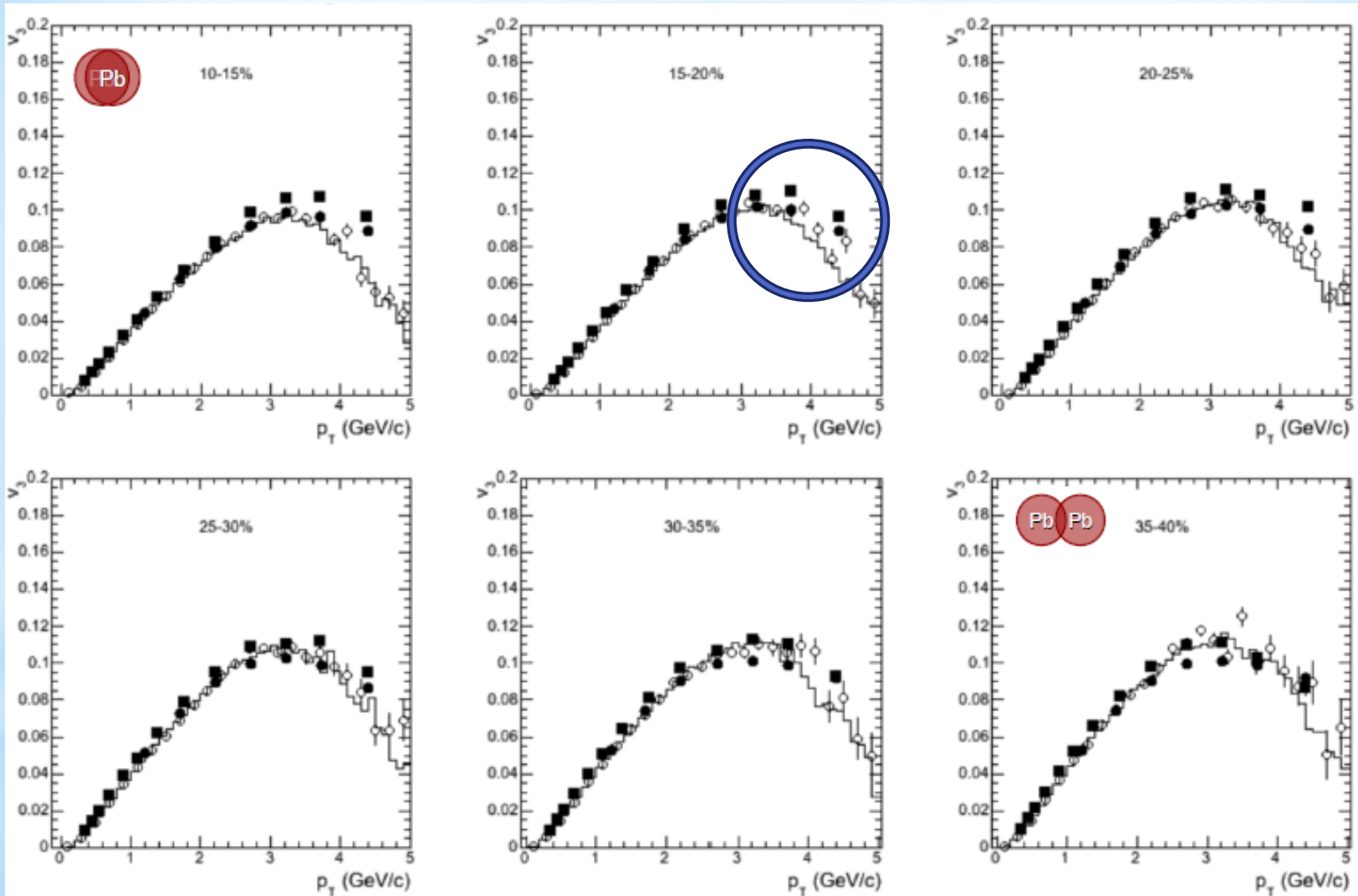
Closed points: CMS data v_2 {2Part & LYZ};

Open points and histograms: HYDJET++ v_2 {EP & Psi2}

LHC data vs. HYDJET++ model

Triangular flow

Pb+Pb @ 2.76 ATeV



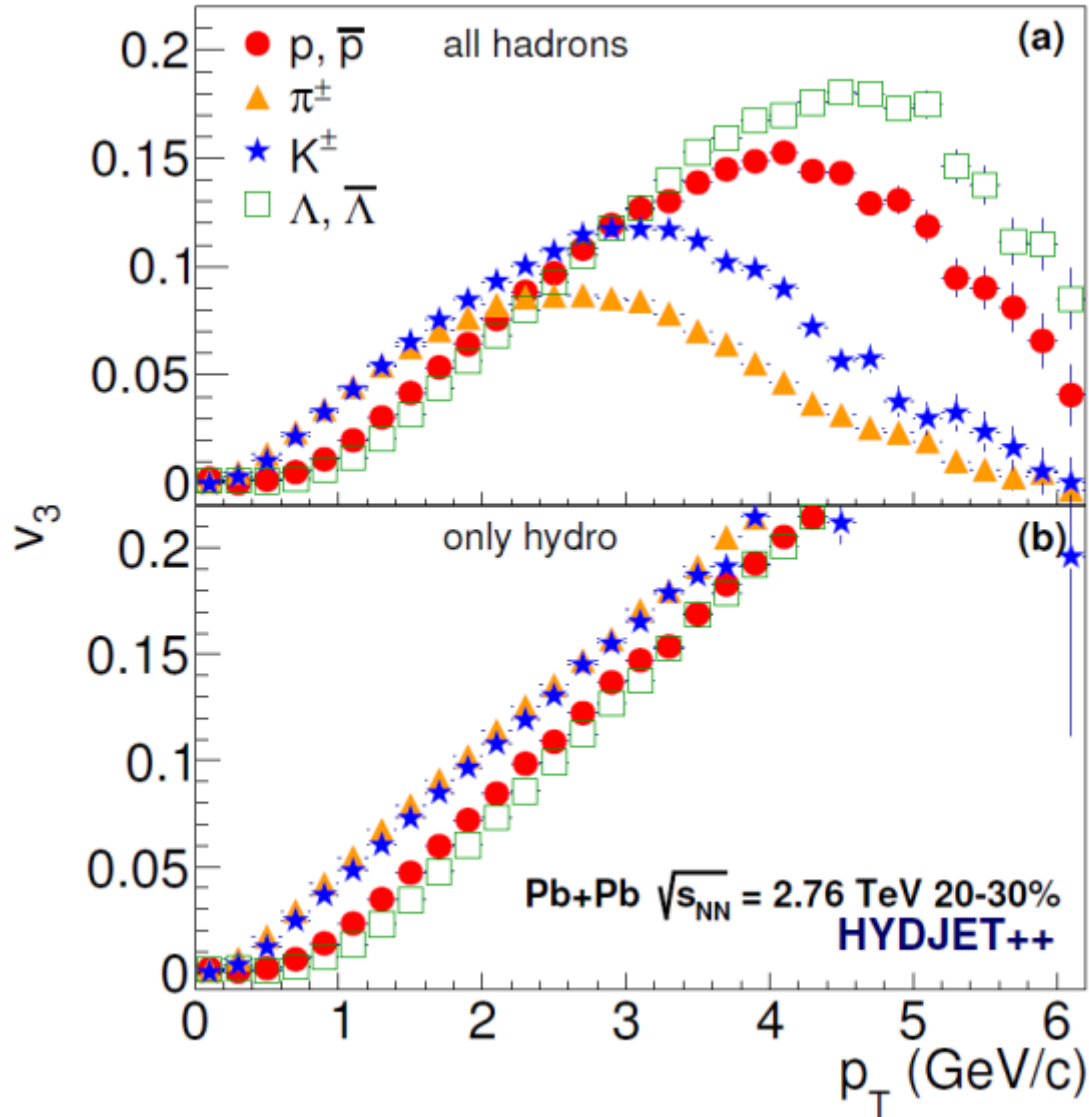
Closed points: CMS data v_2 {2Part & LYZ};

Open points and histograms: HYDJET++ v_2 {EP & Psi3}

Interplay of hydrodynamics and jets

Triangular flow

Pb+Pb @ 2.76 ATeV



Hydrodynamics gives
mass ordering of v_3

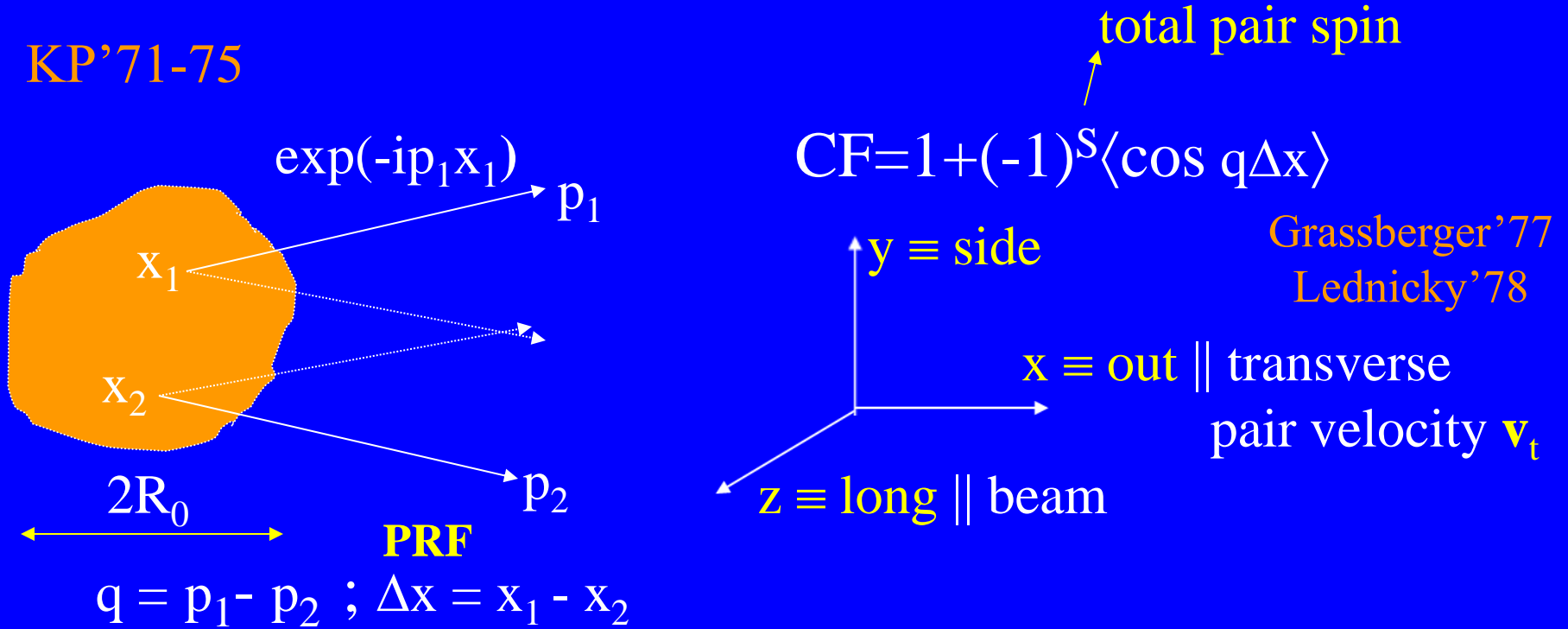
The model possesses
crossing of baryon
and meson branches

The reason for the
mass ordering break
at 2 GeV/c is traced to
hard processes (jets)

III. Femtoscopic correlations

QS symmetrization of production amplitude

→ *momentum correlations of identical particles are sensitive to space-time structure of the source*



$$\langle \cos q \Delta x \rangle = 1 - \frac{1}{2} \langle (q \Delta x)^2 \rangle + \dots \approx \exp(-R_x^2 q_x^2 - R_y^2 q_y^2 - R_z^2 q_z^2 - 2R_{xz}^2 q_x q_z)$$

Femtoscscopy or Interferometry radii:

$$R_x^2 = \frac{1}{2} \langle (\Delta x - v_x \Delta t)^2 \rangle, R_y^2 = \frac{1}{2} \langle (\Delta y)^2 \rangle, R_z^2 = \frac{1}{2} \langle (\Delta z - v_z \Delta t)^2 \rangle$$

Probing source dynamics - expansion

Dispersion of emitter velocities & limited emission momenta (T) \Rightarrow

x-p correlation: interference dominated by pions from nearby emitters

Resonances GKP'71

Strings Bowler'85 ..

\rightarrow Interference probes only a part of the source

\rightarrow Interferometry radii decrease with pair velocity

Hydro Pratt'84,86

Kolehmainen, Gyulassy'86

Makhlin-Sinyukov'87

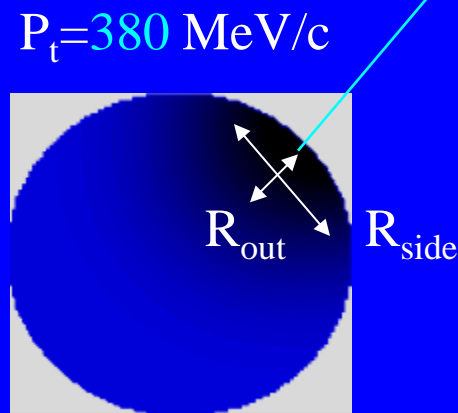
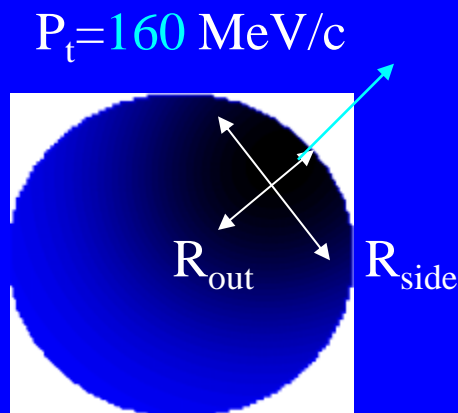
Bertch, Gong, Tohyama'88

Hama, Padula'88

Pratt, Csörgö, Zimanyi'90

Mayer, Schnedermann, Heinz'92

.....



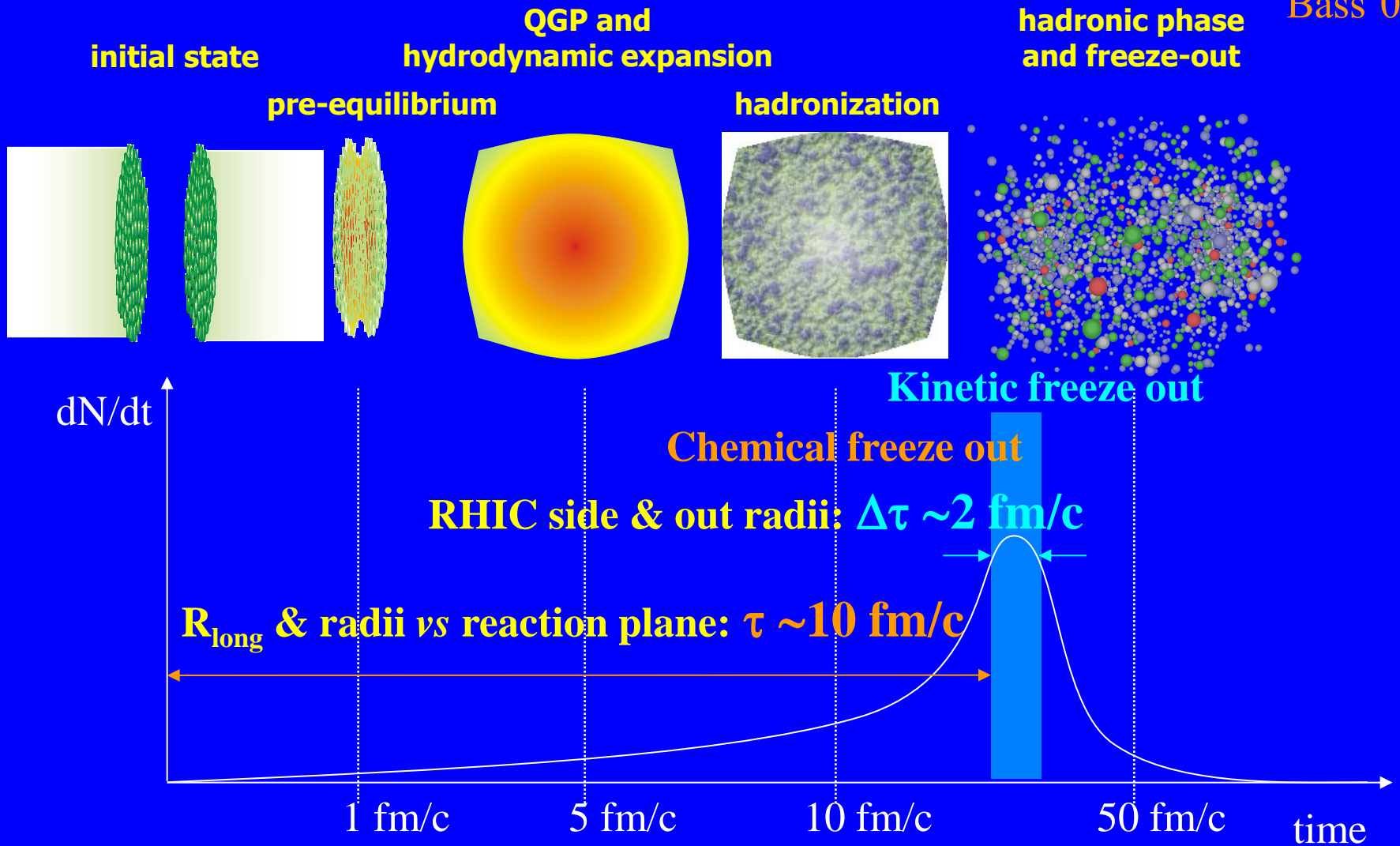
Collective transverse flow $\beta^F \rightarrow R_{side} \approx R / (1 + m_t \beta^{F2} / T)^{1/2}$

in LCMS: 1

Longitudinal boost invariant expansion during proper freeze-out (evolution) time $\tau \rightarrow R_{long} \approx (T/m_t)^{1/2} \tau / \cosh y$

Expected evolution of HI collision vs RHIC data

Bass'02



**IV. Geometric and dynamical
anisotropy:
consequences for flow and
radii**

Results: Phenix paper

Angular dependence of radii fit with:

$$R_\mu^2 = R_0^2 + 2 \sum_{n=m,2m} R_{\mu,n}^2 \cos[n(\phi - \Psi_m)] \quad (\mu = s, o, l)$$

$$R_\mu^2 = 2 \sum_{n=m,2m} R_{\mu,n}^2 \sin[n(\phi - \Psi_m)] \quad (\mu = os)$$

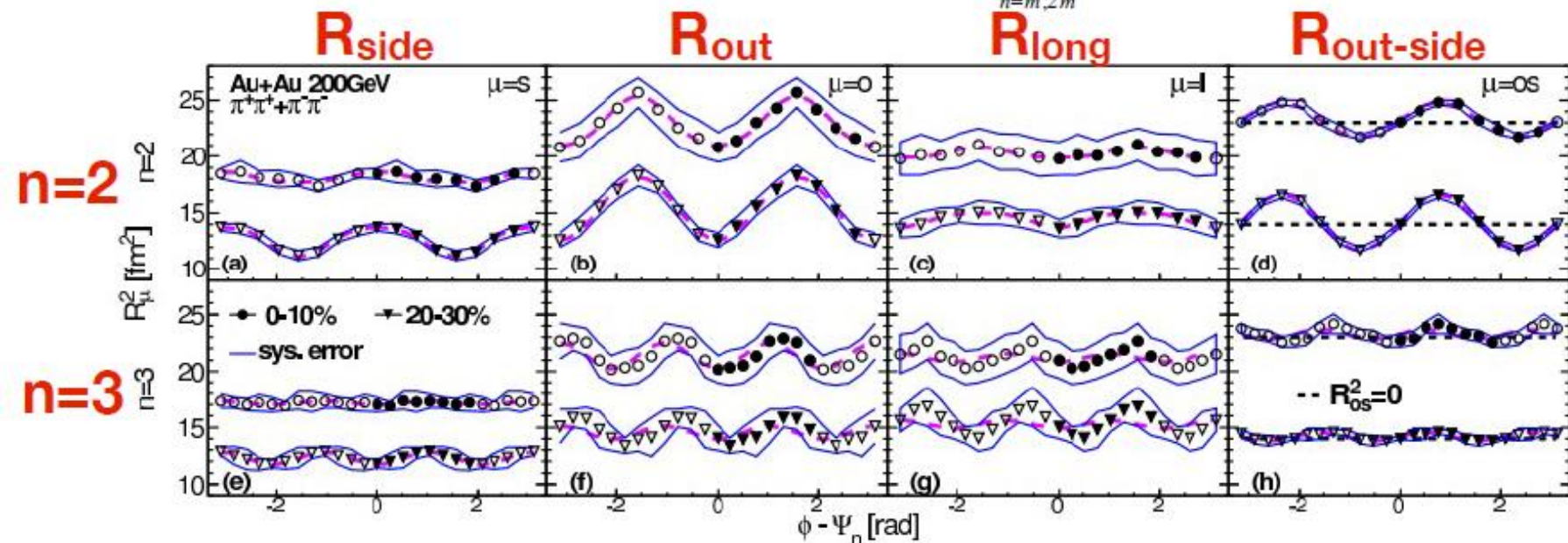


FIG. 1: (Color online) The azimuthal dependence of R_s^2 , R_o^2 , R_l^2 , and R_{os}^2 for charged pions in $0.2 < k_T < 2.0$ GeV/c with respect to 2nd (a-d) and 3rd-order (e-h) event plane in Au+Au collisions at $\sqrt{s_{NN}} = 200$ GeV. The R_{os}^2 is plotted relative to dashed lines representing $R_{os}^2 = 0$. The filled symbols show the extracted HBT radii and the open symbols are reflected by symmetry around $\phi - \Psi_n = 0$. Bands of two thin lines show the systematic uncertainties and dashed lines show the fit lines by Eq. (3).

0 – 10% : R_s^2 shows a weak oscillation for Ψ_2, Ψ_3

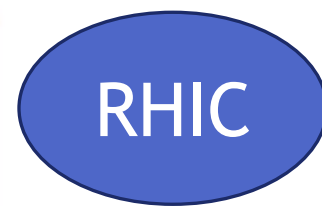
R_o^2 shows a strong oscillation for Ψ_2, Ψ_3

20 – 30% : R_s^2 & R_o^2 shows opposite oscillation for Ψ_2

R_s^2 shows a weak oscillation with same sign for Ψ_3

V. Loggins Wayne State University

ALICE PHYSICS CLUB Page 8



WAYNE STATE
UNIVERSITY



Summary 1: Gaussian Toy Model

Plumberg, Chun, & Heinz Phys. Rev. C **88**, 044914 (2013)

- Do we understand the third order HBT oscillation?

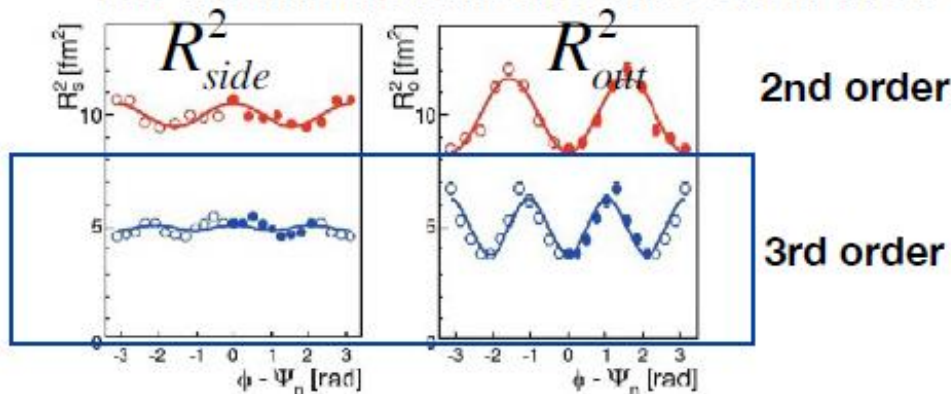


FIG. 2. (Color online) Second- and third-order oscillations of R_{side}^2 and R_{out}^2 measured by the PHENIX Collaboration in central (0%–10%) 200 A GeV Au + Au collisions [13]. For better visibility, the average values $R_{s,o}^2$ of the two radius parameters were set by hand to 5 and 10 fm², respectively, when plotting the third- and second-order oscillations.

Deformed flow field simulation (blue) is in agreement with data

Deformed geometry field simulation (red) does not follow data

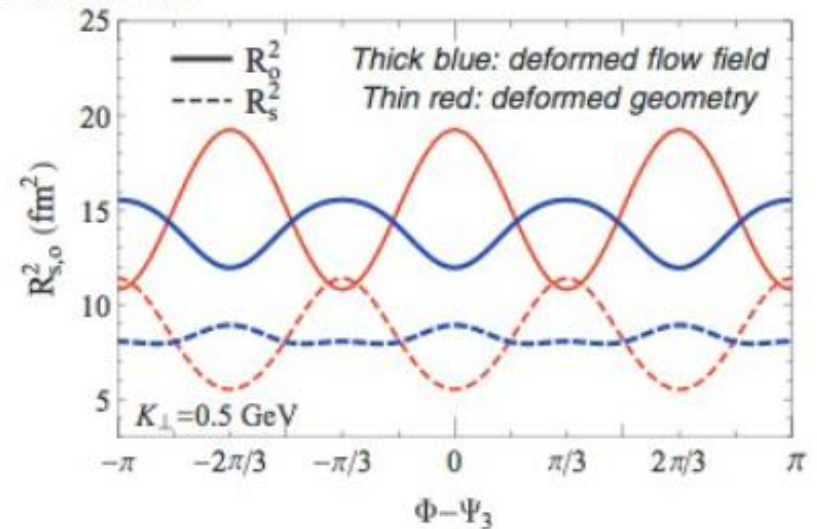
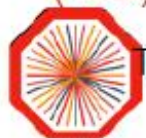


FIG. 3. (Color online) Triangular oscillations of R_s^2 (dashed) and R_o^2 (solid) for pion pairs with momentum $K_{\perp} = 0.5$ GeV, as a function of emission angle Φ relative to the triangular flow direction Ψ_3 . Shown are results for two model scenarios: A deformed flow field ($\bar{v}_3 = 0.25$) in a spatially isotropic ($\bar{\epsilon}_3 = 0$) density distribution (thick blue lines), and a source with triangular geometric deformation ($\bar{\epsilon}_3 = 0.25$) expanding with radially symmetric ($\bar{v}_3 = 0$) flow (thin red lines). For the two scenarios the oscillations of both R_s^2 and R_o^2 are seen to be out of phase by $\pi/3$.

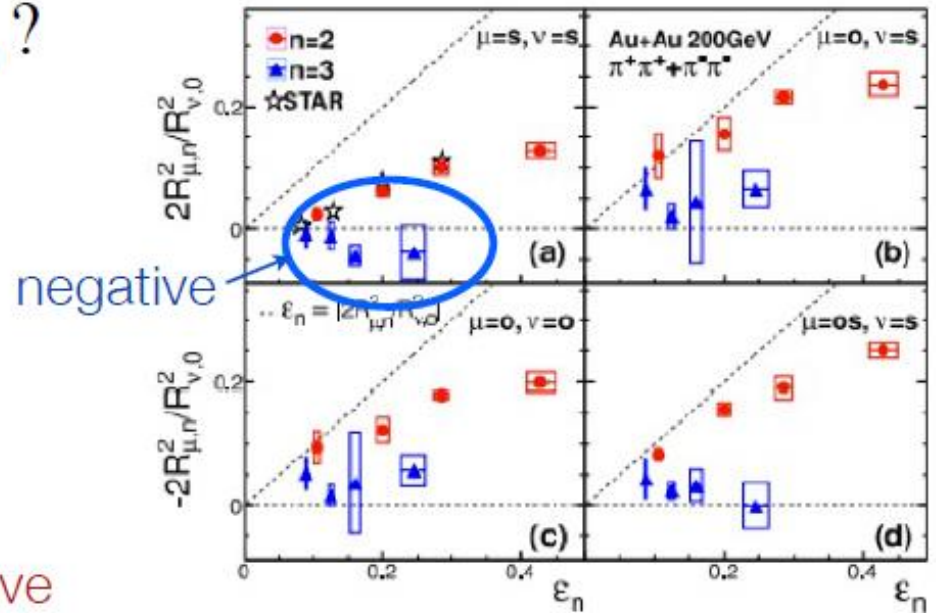
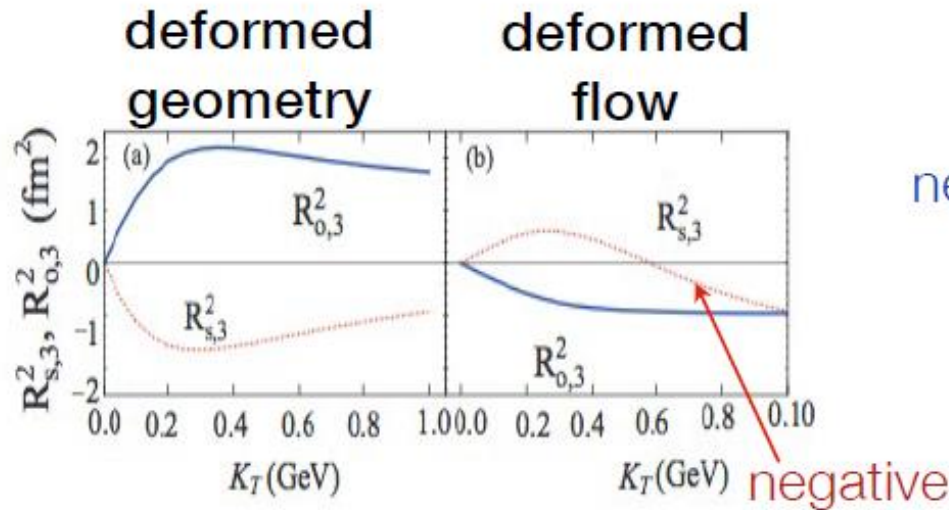


This compliments PHENIX figure 3 & MC simulation

Summary 1: Gaussian Toy Model

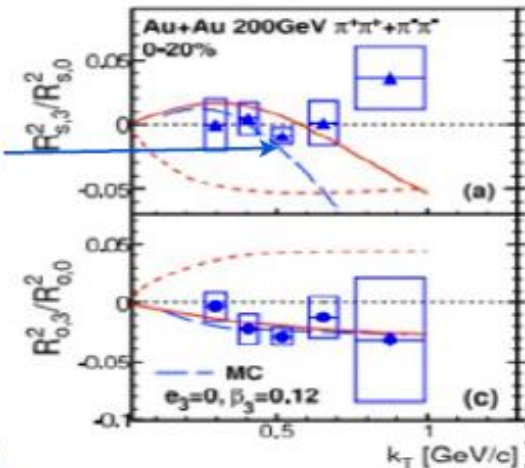
Plumberg, Chun, & Heinz Phys. Rev. C **88**, 044914 (2013)

Do we understand $2R_{s,3}^2/R_{s,0}^2$?



$R_{s,3}^2$ goes negative for the deformed flow case,

this may be why $2R_{s,3}^2/R_{s,0}^2$ may be less than negative equal to zero.



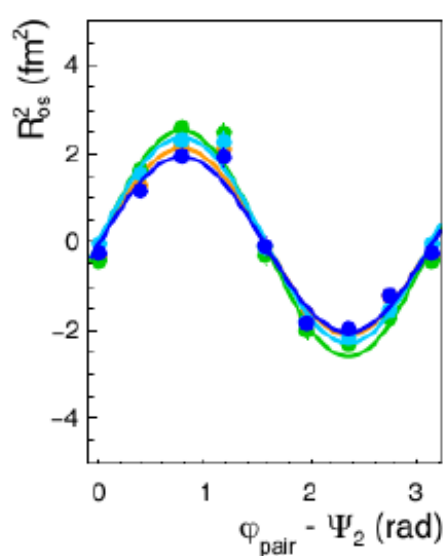
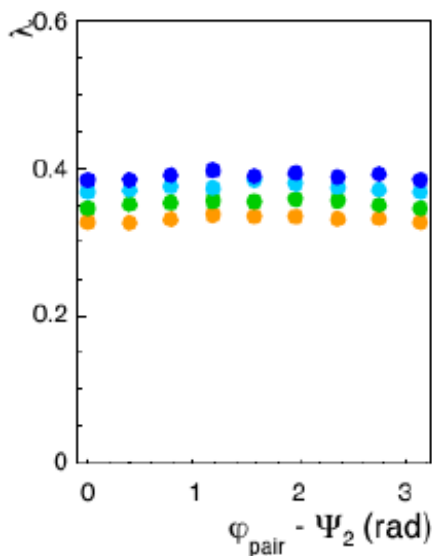
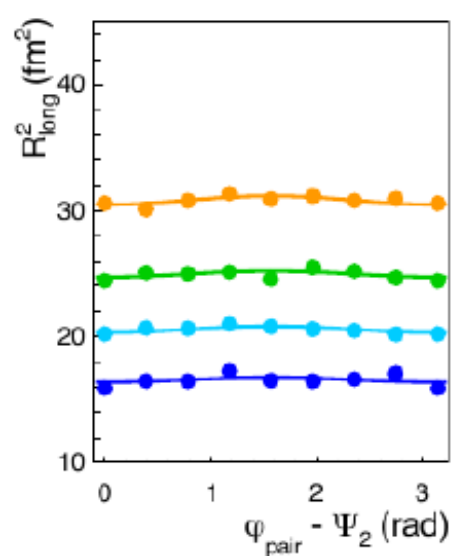
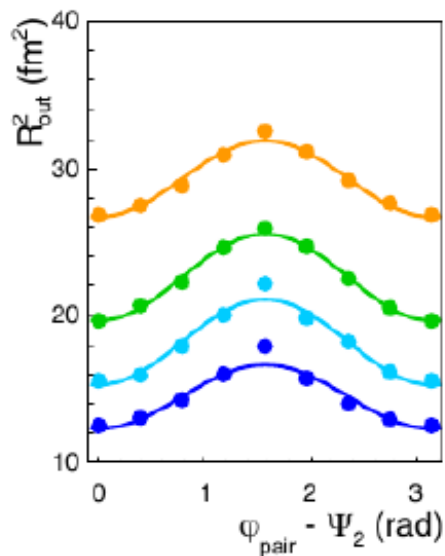
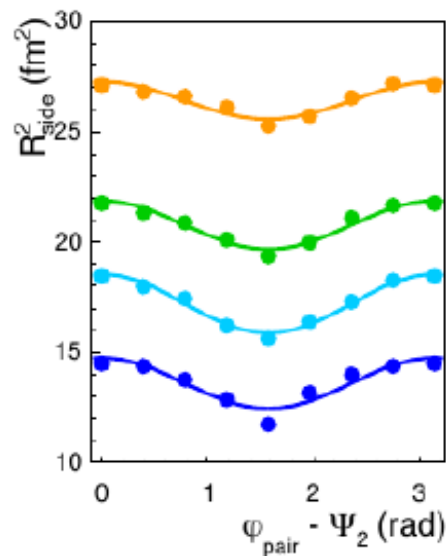
STATE
UNIVERSITY



Azimuthally sensitive HBT radii w.r.t. Ψ_2

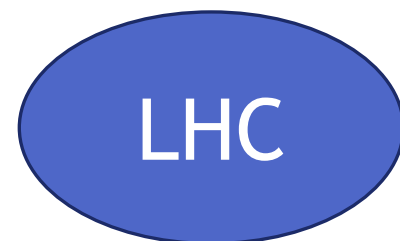
$k_T: 0.2-2.0(\text{GeV}/c)$

Ψ_2 is measured via FMD A+C



centrality

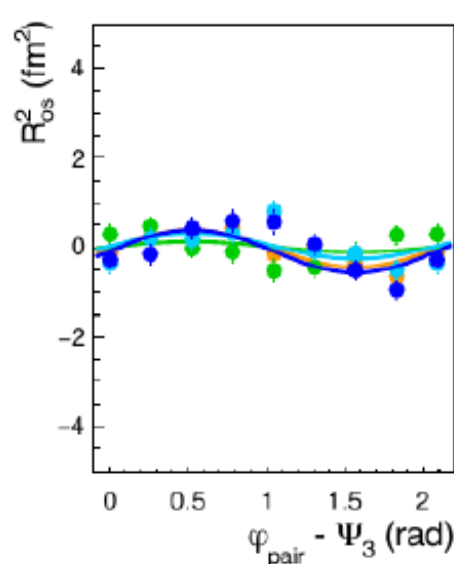
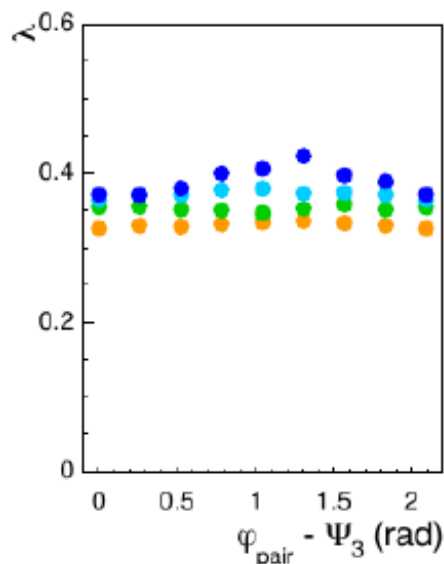
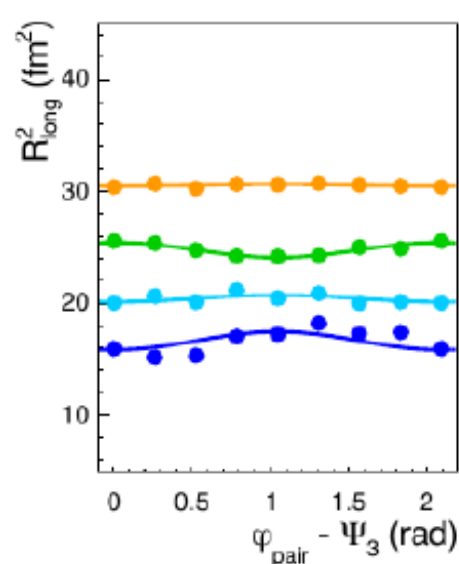
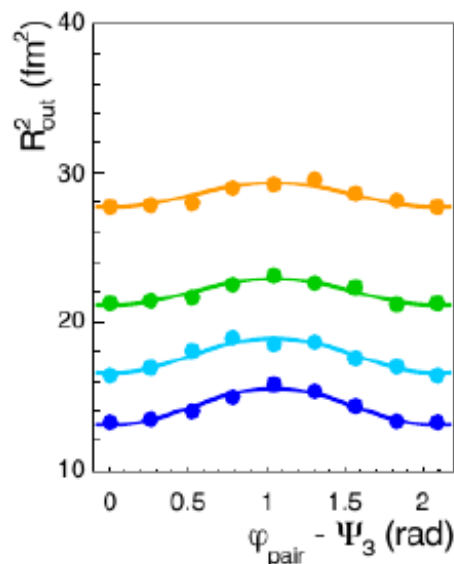
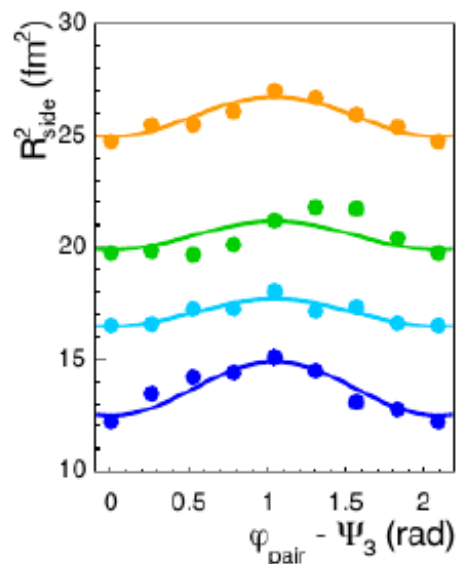
- 0-5%
- 5-10%
- 10-20%
- 20-30%
- 30-40%
- 40-50%



Azimuthally sensitive HBT radii w.r.t. Ψ_3

kT:0.2-2.0(GeV/c)

Ψ_3 is measured via FMD A+C



centrality

—●— 10-20%

—●— 20-30%

—●— 30-40%

—●— 40-50%

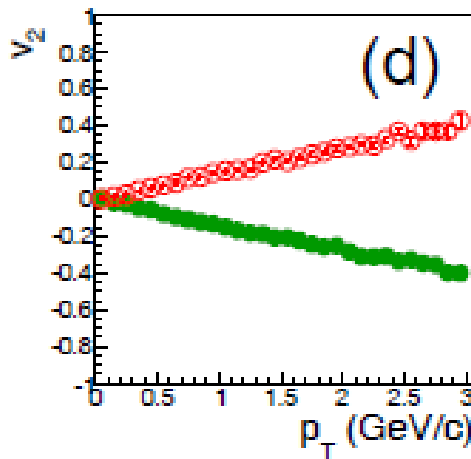
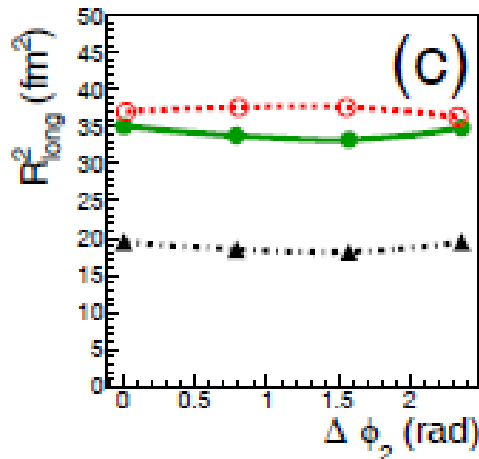
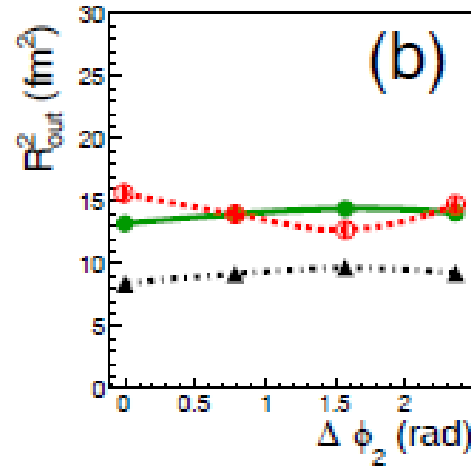
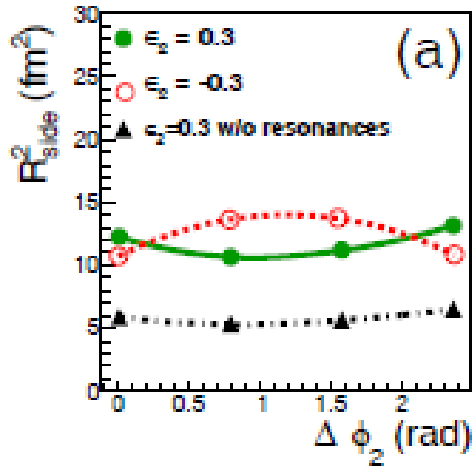
V. Simultaneous description of the flow and HBT radii

Spatial vs Dynamical Anisotropy

L. Bravina et al., Eur.Phys.J. A53 (2017) 219 / arXiv: 1709.08602 [hep-ph]

Elliptic flow and radii oscillations w.r.t. Ψ_2 plane

Pb+Pb @ 2.76 TeV



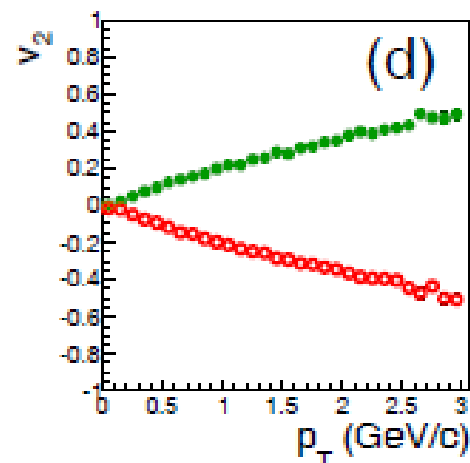
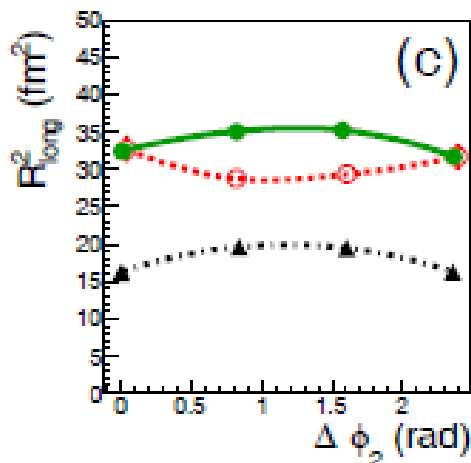
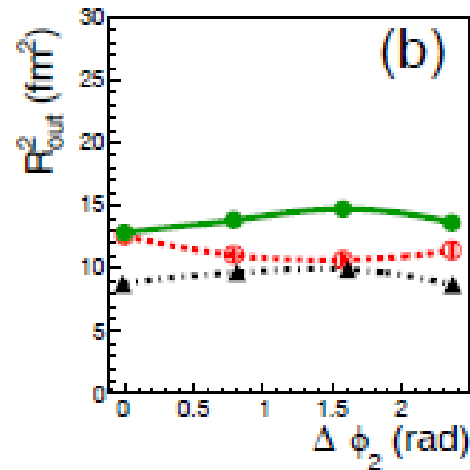
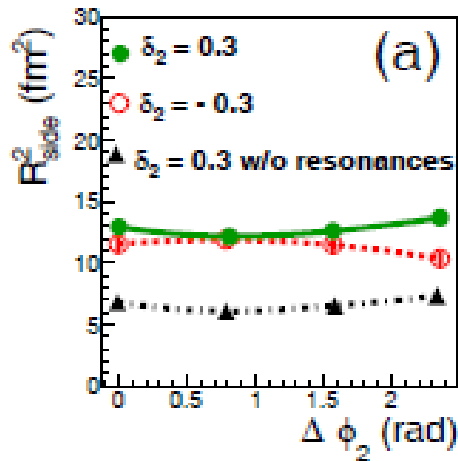
$$\epsilon_2 = \pm 0.3$$

Other anisotropy parameters are zero (only spatial anisotropy).

Either flow or radii oscillations !?

Spatial vs Dynamical Anisotropy

Elliptic flow and radii oscillations w.r.t. Ψ_2 plane



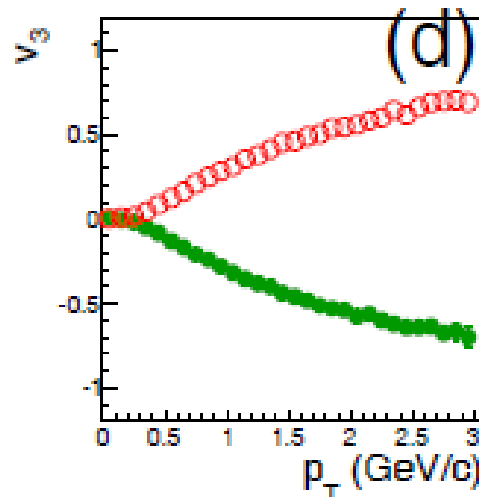
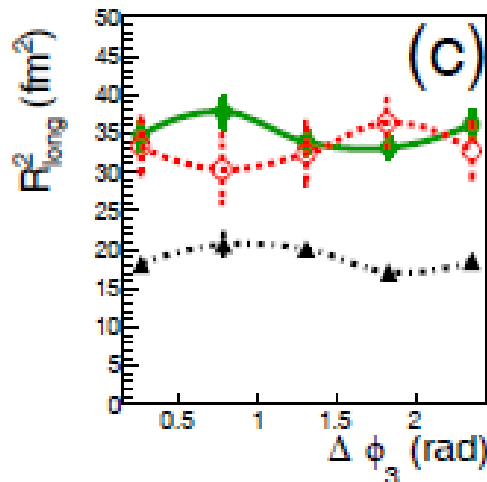
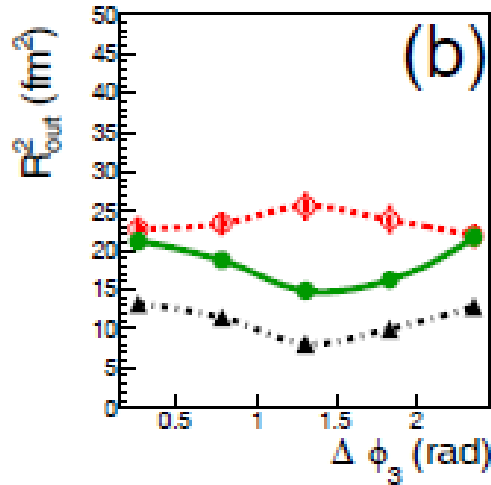
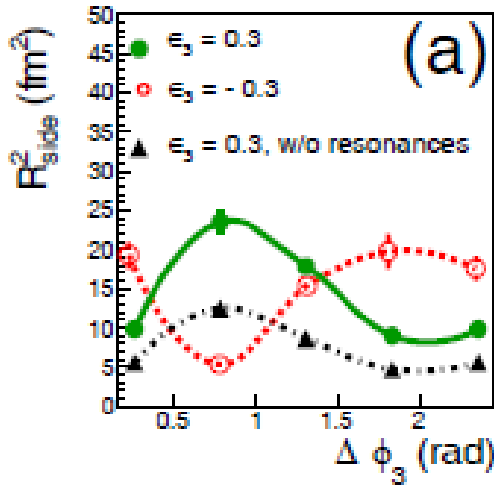
$$\delta_2 = \pm 0.3$$

Other anisotropy parameters are zero (only dynamical anisotropy).

Correct v_2 and oscillation phases for $\delta_2 > 0$

Spatial vs Dynamical Anisotropy

Triangular flow and radii oscillations w.r.t. Ψ_3 plane



$$\epsilon_3 = \pm 0.3$$

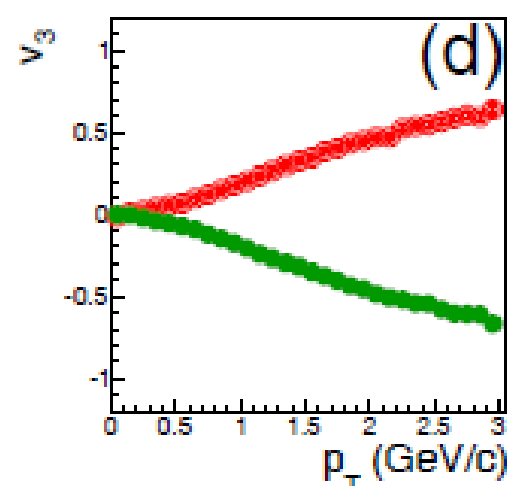
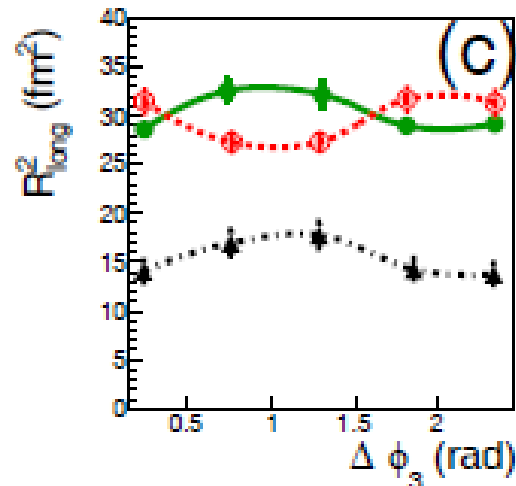
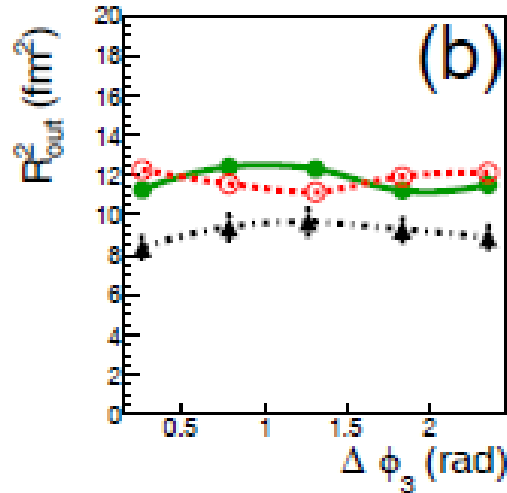
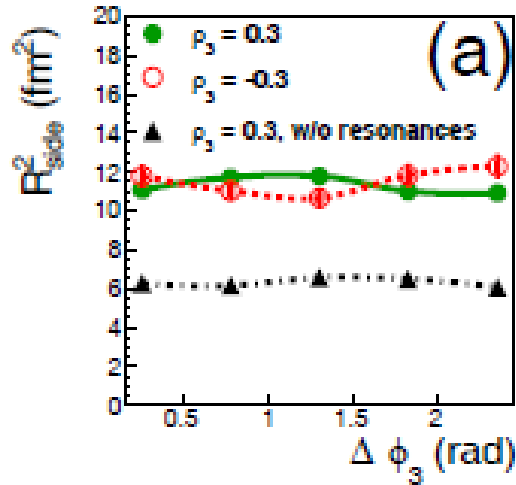
Other anisotropy parameters are zero

(only spatial anisotropy).

Again, either flow or radii oscillations are reproduced

Spatial vs Dynamical Anisotropy

Triangular flow and radii oscillations w.r.t. Ψ_3 plane



$$\rho_3 = \pm 0.3$$

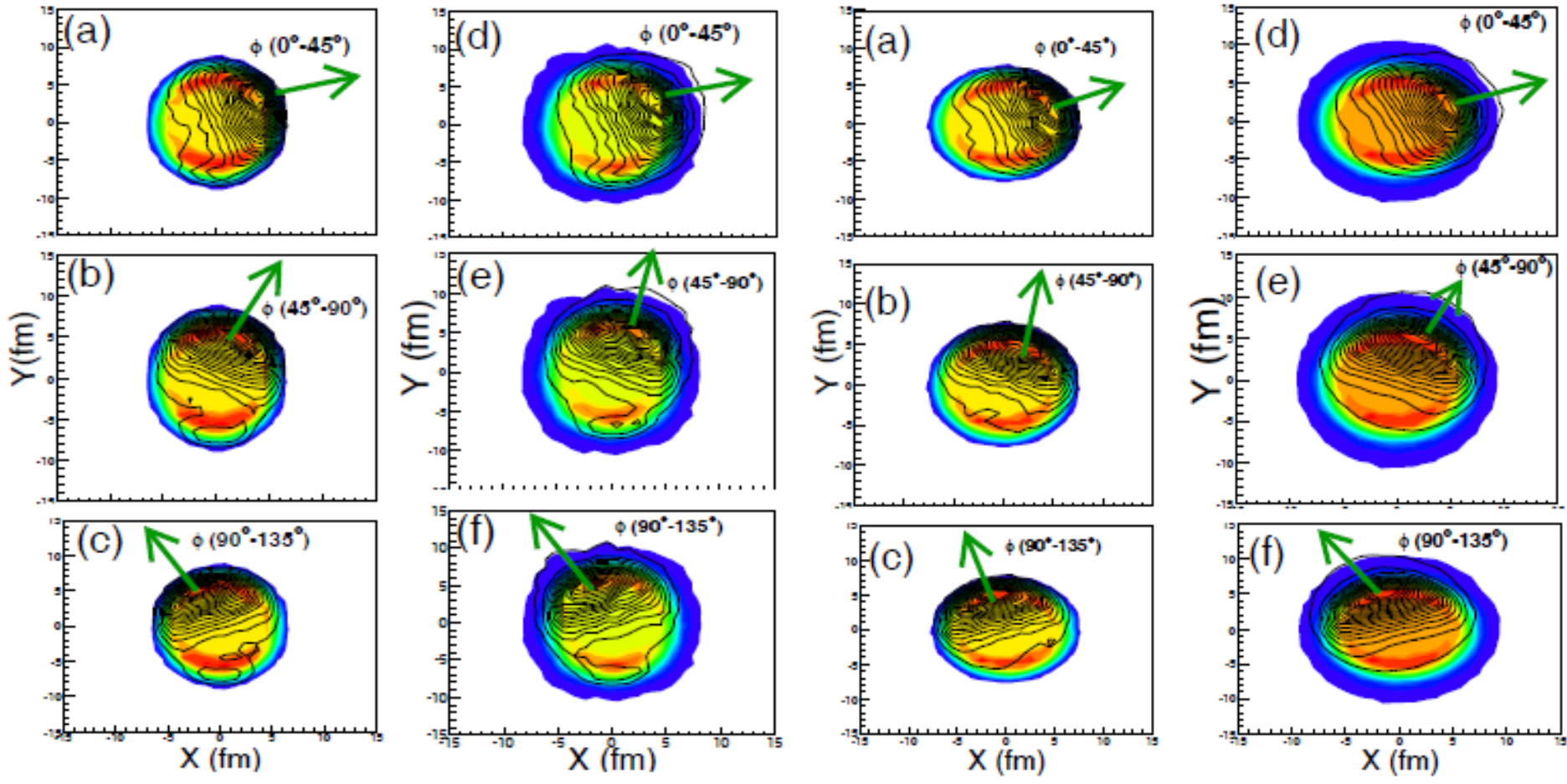
Other anisotropy parameters are zero (only dynamical anisotropy).

Correct v_3 and oscillation phases for $\rho_3 > 0$

Spatial vs Dynamical Anisotropy. Influence of resonance decays

Spatial

Dynamical

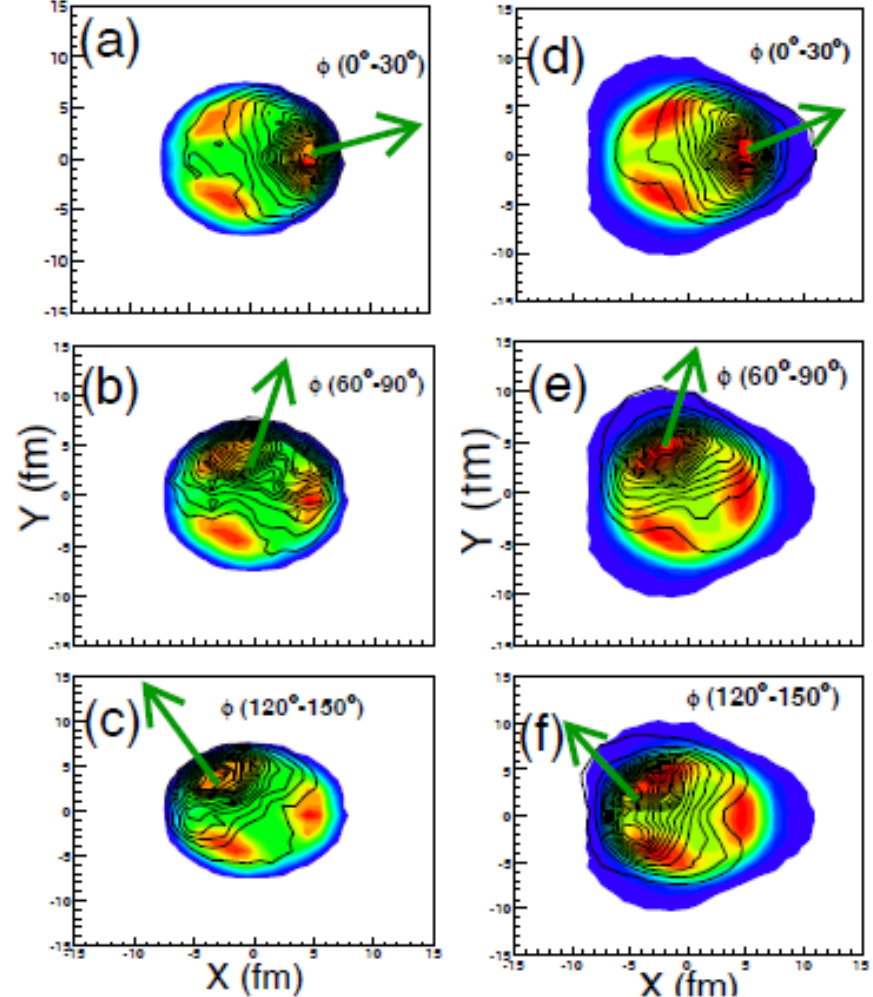
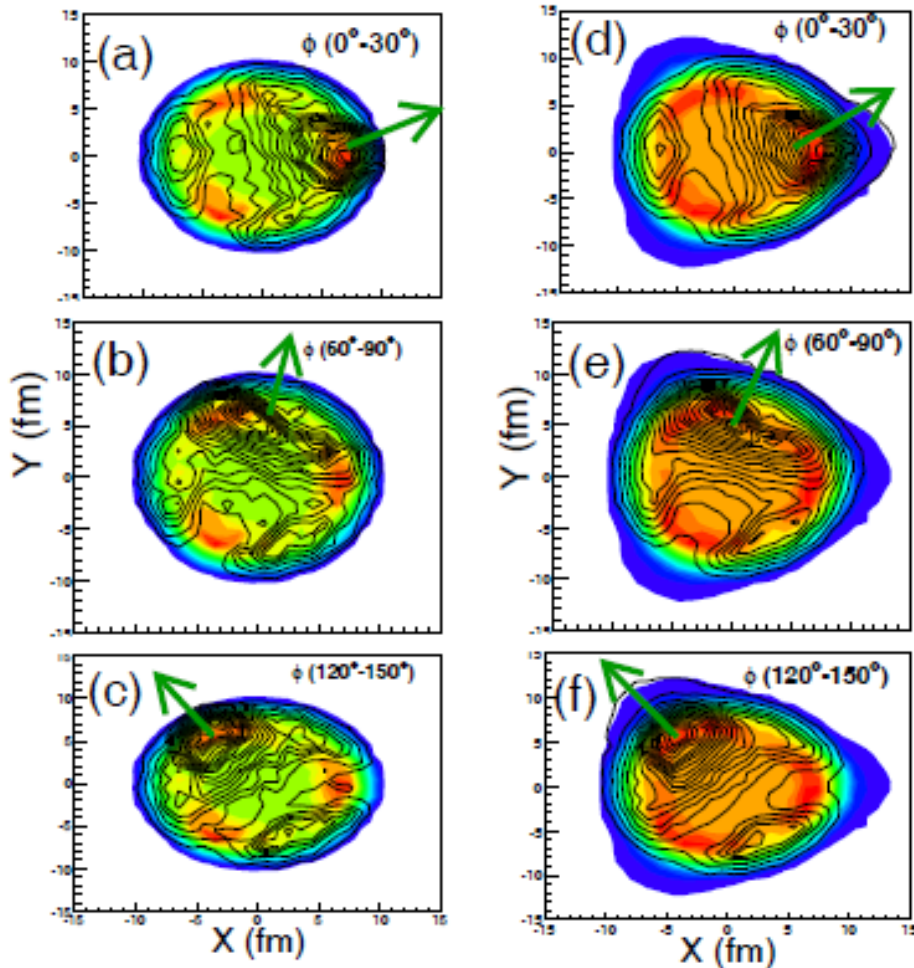


Elliptic anisotropy

Spatial vs Dynamical Anisotropy. Influence of resonance decays

Spatial

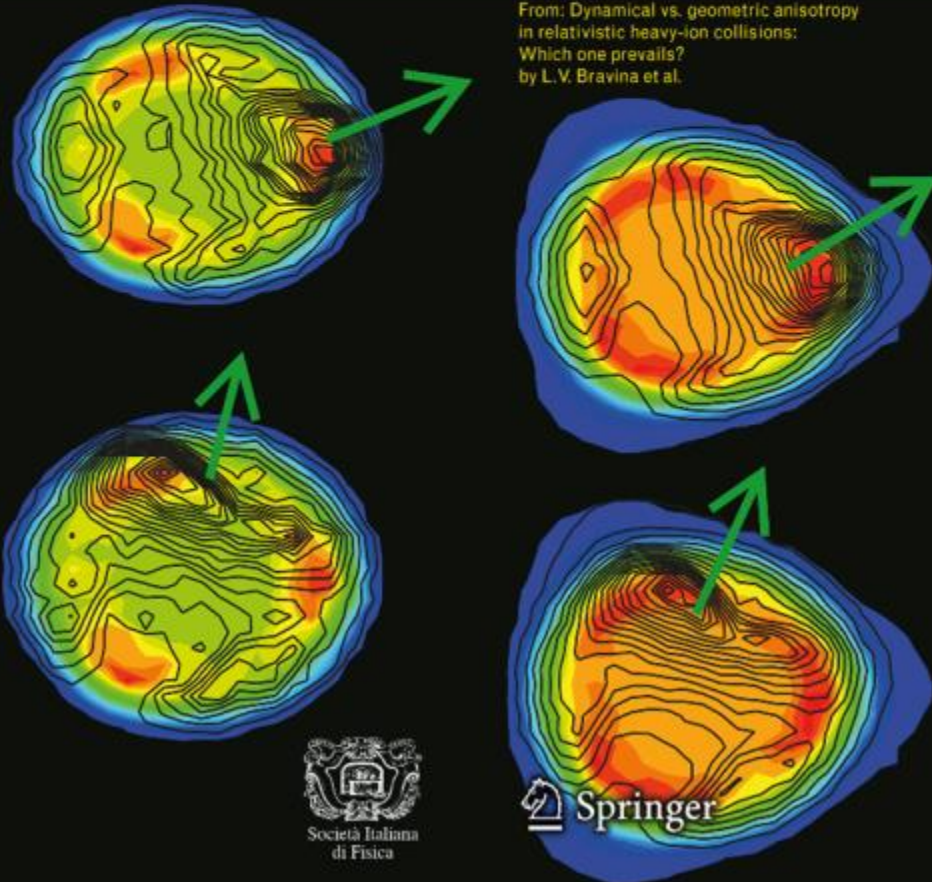
Dynamical



Triangular anisotropy



From: Dynamical vs. geometric anisotropy
in relativistic heavy-ion collisions:
Which one prevails?
by L. V. Bravina et al.



**L.V. Bravina,
I.P. Lokhtin,
L.V. Malinina,
S.V. Petrushanko,
A.M. Snigirev,
E.E. Zabrodin,
"Dynamical vs. geometric
anisotropy in relativistic
heavy-ion collisions: Which
one prevails?",
Eur. Phys. J. A 53 (2017) 219.**

CONCLUSIONS

Second- and third-order oscillations of the femtoscopic radii in Pb+Pb collisions at 2.76 TeV were studied within the HYDJET++ model together with the differential elliptic and triangular flow. Our study indicates that

- *Elliptic or triangular spatial anisotropy alone cannot reproduce simultaneously the correct phase of the radii oscillations and the correct sign of the corresponding flow harmonics*
- *Dynamical flow anisotropy provides correct **qualitative** description of both P_T -dependence of v_2 and v_3 and the phases of the femtoscopic radii oscillations*
- *Decays of resonances provide significant increase of the emitting areas and make the radii oscillations more pronounced*
- *However, they do not change the phases of the oscillations*
- *Both spatial and dynamical anisotropy is needed for the **quantitative** description of both signals.*

Back-up Slides

HYDJET++ (soft): thermal and chemical freeze-outs

1. The particle densities at the **chemical freeze-out** stage are too high to consider particles as free streaming and to associate this stage with the **thermal freeze-out**

2. Within the concept of chemically frozen evolution, the conservation of the particle number ratios from the chemical to thermal freeze-out is assumed:

$$\frac{\rho_i^{eq}(T^{ch}, \mu_i^{ch})}{\rho_\pi^{eq}(T^{ch}, \mu_\pi^{ch})} = \frac{\rho_i^{eq}(T^{th}, \mu_i^{th})}{\rho_\pi^{eq}(T^{th}, \mu_\pi^{th})}$$

3. The absolute values of $\rho_i^{eq}(T^{th}, \mu_i^{th})$ are determined by the choice of the **free parameter of the model: effective pion chemical potential** $\mu_\pi^{eff,th}$ at T^{th} . For hadrons heavier than pions the Boltzmann approximation is assumed:

$$\mu_i^{th} = T^{th} \ln \left(\frac{\rho_i^{eq}(T^{ch}, \mu_i^{ch})}{\rho_i^{eq}(T^{th}, \mu_i = 0)} \frac{\rho_\pi^{eq}(T^{th}, \mu_\pi^{eff,th})}{\rho_\pi^{eq}(T^{ch}, \mu_i^{ch})} \right)$$

Particle momentum spectra are generated on the **thermal freeze-out hypersurface**, the hadronic composition at this stage is defined by the parameters of the system at chemical freeze-out

HYDJET++ (hard): PYQUEN (PYthia QUENched)

Initial parton configuration
PYTHIA Q20 w/o hadronization: `mstp(111)=0`



Parton rescattering & energy loss (collisional, radiative) + emitted g
PYQUEN rearranges partons to update ns strings

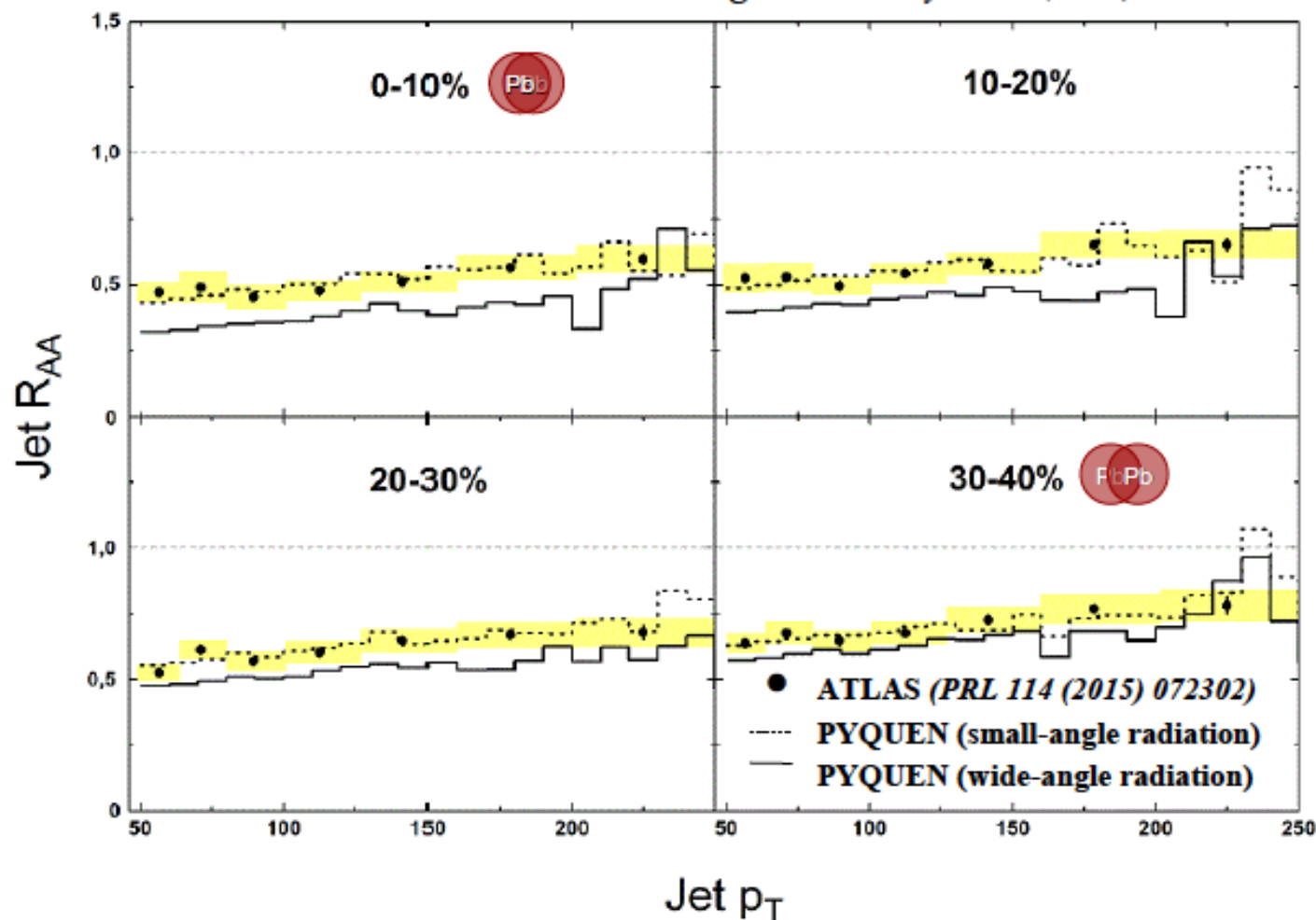


Parton hadronization and final particle formation
PYTHIA Q20 with hadronization: call PYEXEC

Three model parameters: initial QGP temperature T_0 , QGP formation time τ_0 and
number of active quark flavors in QGP N_f
(+ minimal pT of hard process P_{tmin})

Suppression factor of inclusive jets vs P_T in PYQUEN at LHC

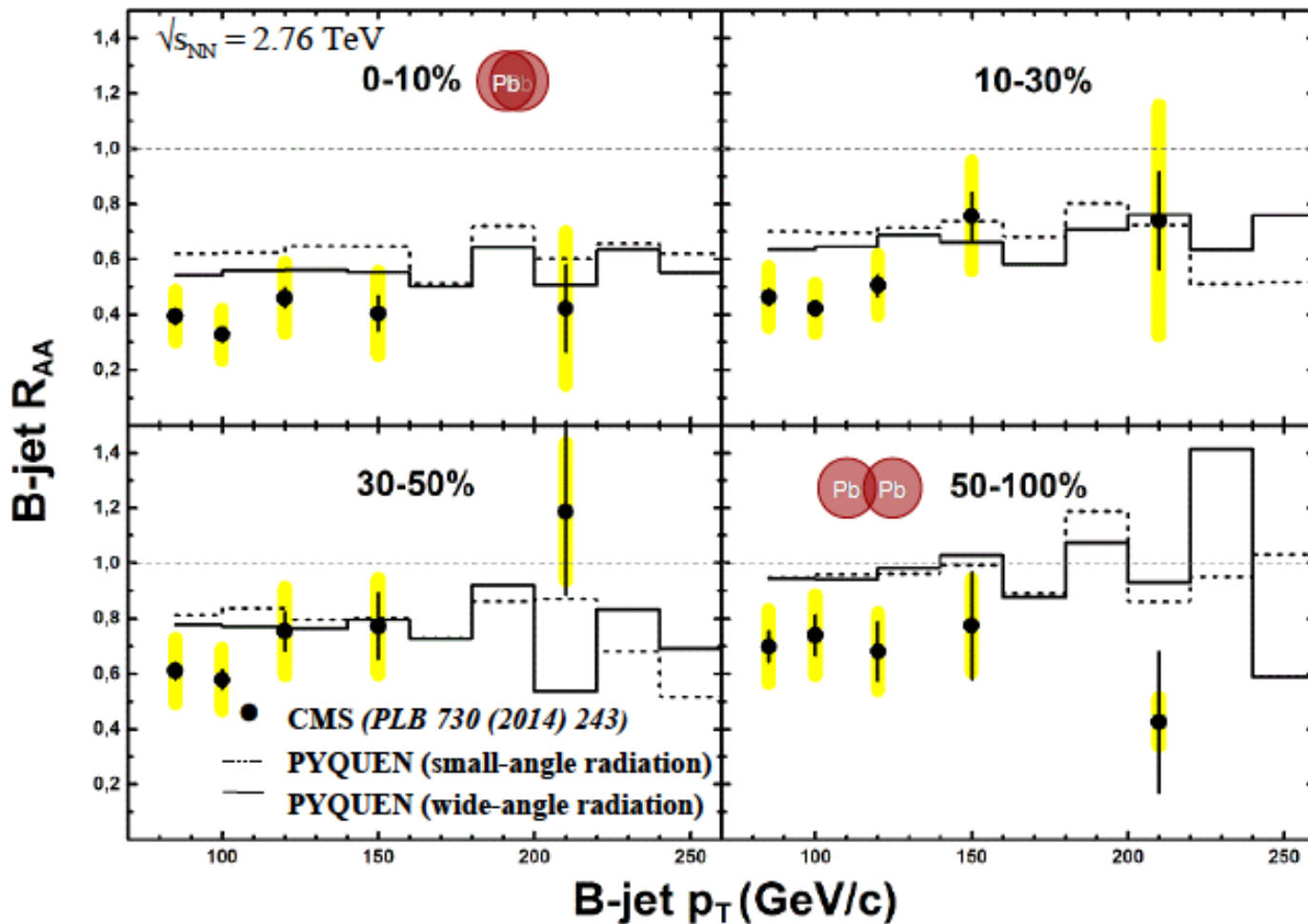
I.P. Lokhtin, A.A. Alkin, A.M. Snigirev, Eur.Phys. J. C (2015) 75



PYQUEN simulation results for R_{AA} are close to the data within statistical and systematic experimental uncertainties.

Suppression factor of b-jets vs. p_T in CMS and PYQUEN

I.P. Lokhtin, A.A. Alkin, A.M. Snigirev, Eur.Phys. J. C (2015) 75



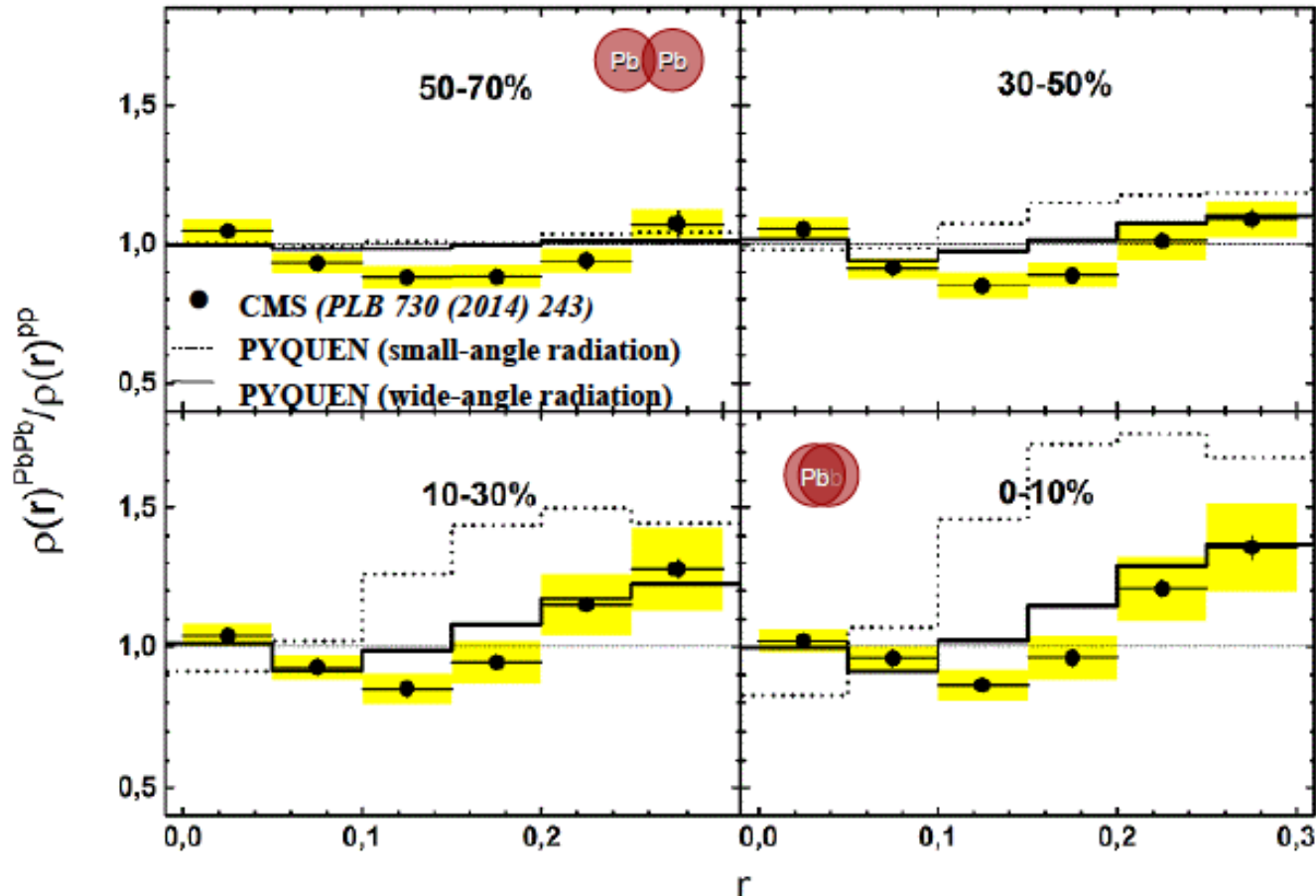
Reproduced well by PYQUEN



Jet shapes PYQUEN vs. CMS data

$$\rho(r) \sim \frac{1}{\delta r} \frac{1}{N_{\text{jet}}} \sum_{\text{jets}} \frac{p_T(r - \delta r/2, r + \delta r/2)}{p_T^{\text{jet}}} \quad \text{二十五}$$

I.P. Lokhtin, A.A. Alkin, A.M. Snigirev, Eur.Phys. J. C (2015) 75

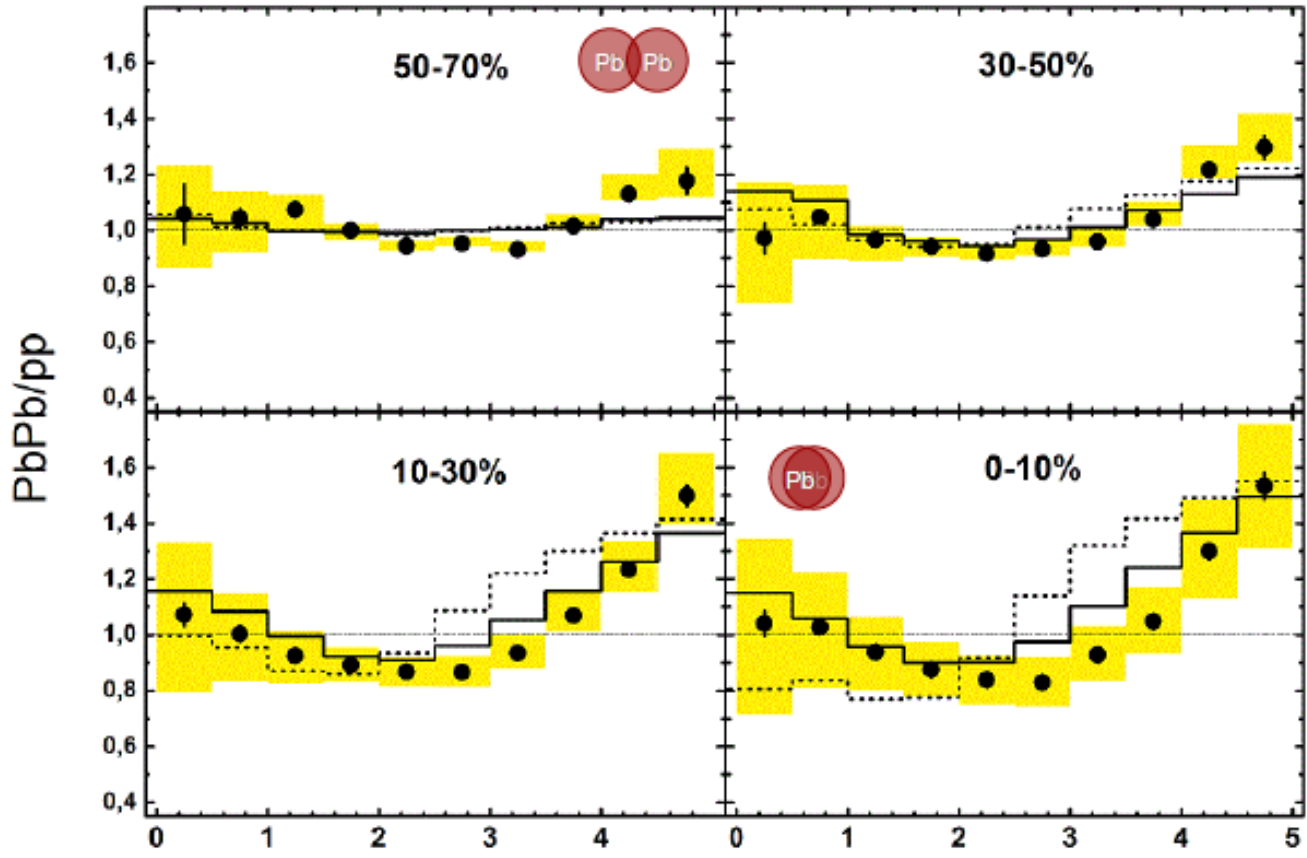


The modification of radial jet profile ($E_T^{\text{jet}} > 100$ GeV, $R=0.3$): excess at large radii; suppression at intermediate radii; core is unchanged. Reproduced well by PYQUEN with wide-angle radiative + collisional partonic energy loss.

Jet fragmentation function PYQUEN vs. CMS data

$$\zeta = -\ln z = -\ln \frac{p_T^{track}}{p_T^{jet}}$$

I.P. Lokhtin, A.A. Alkin, A.M. Snigirev, Eur.Phys. J. C (2015) 75



$$\xi = \ln(1/z)$$

The modification of longitudinal jet profile ($E_T^{jet} > 100$ GeV, $R=0.3$): excess at low p_T ; suppression at intermediate p_T ; high p_T is slightly enhanced. Reproduced well by PYQUEN with wide-angle radiative + collisional partonic energy loss.

Sergey Petrushanko

HYDJET++ model

莫斯科国立大学



Thermal production

- Hadrons are produced on the freeze-out hypersurface with particle density ρ and effective volume V_{eff} . Multiplicities are defined with T^{ch} for stable hadrons and resonances:

$$\overline{N}_i = \rho_i(T, \mu_i) V_{\text{eff}} \quad P(N_i) = \exp(-\overline{N}_i) \frac{(\overline{N}_i)^{N_i}}{N_i!}$$

Mean multiplicity EbE distribution

- Momentum distribution is defined with T^{th} .

$$f_i^{\text{eq}}(p^{*0}, T^{\text{th}}, \mu_i, \gamma_s) = \frac{g_i}{\gamma_s^{-n_i^s} \exp([p^{*0} - \mu_i]/T^{\text{th}}) \pm 1}$$

Momentum distribution function in the fluid element rest frame

- Decay kinematics is taken into account.
- The final hadron spectrum are given by the superposition of thermal distribution and collective flow of fireball liquid assuming Bjorken's scaling.

PYQUEN: physics frames

General kinetic integral equation:

$$\Delta E(L, E) = \int_0^L dx \frac{dP}{dx}(x) \lambda(x) \frac{dE}{dx}(x, E), \quad \frac{dP}{dx}(x) = \frac{1}{\lambda(x)} \exp(-x/\lambda(x))$$

1. Collisional loss and elastic scattering cross section:

$$\frac{dE}{dx} = \frac{1}{4\Gamma\lambda\sigma} \int_{\mu_D^2}^{t_{\max}} dt \frac{d\sigma}{dt} t, \quad \frac{d\sigma}{dt} \simeq C \frac{2\pi\alpha_s^2(t)}{t^2}, \quad \alpha_s = \frac{12\pi}{(33-2N_f) \ln(t/\Lambda_{QCD}^2)}, \quad C = 9/4(\%gg), 1(gq), 4/9(qq)$$

2. Radiative loss (BDMS):

$$\frac{dE}{dx}(m_q=0) = \frac{2\alpha_s C_F}{\pi\tau_L} \int_{E_{LPM} \sim \lambda_g \mu_D^2}^E d\omega \left[1 - y + \frac{y^2}{2} \right] \ln |\cos(\omega_1 \tau_1)|, \quad \omega_1 = \sqrt{i \left(1 - y + \frac{C_F}{3} y^2 \right) \bar{k} \ln \frac{16}{\bar{k}}}, \quad \bar{k} = \frac{\mu_D^2 \lambda_g}{\omega(1-y)}, \quad \tau_1 = \frac{\tau_L}{2\lambda_g}, \quad y = \frac{\omega}{E}, \quad C_F = \frac{4}{3}$$

“dead cone” approximation for massive quarks:

$$\frac{dE}{dx}(m_q \neq 0) = \frac{1}{(1+(l\omega)^{3/2})^2} \frac{dE}{dx}(m_q=0), \quad l = \left(\frac{\lambda}{\mu_D^2} \right)^{1/3} \left(\frac{m_q}{E} \right)^{4/3}$$

Monte-Carlo simulation of parton rescattering and energy loss in PYQUEN

- Distribution over jet production vertex $V(r \cos \psi, r \sin \psi)$ at im.p. b

$$\frac{dN}{d\psi dr}(b) = \frac{T_A(r_1)T_A(r_2)}{\int_0^{2\pi} d\psi \int_0^{r_{max}} r dr T_A(r_1)T_A(r_2)}$$

- Transverse distance between parton scatterings $l_i = (\tau_{i+1} - \tau_i) E/p_T$

$$\frac{dP}{dl_i} = \lambda^{-1}(\tau_{i+1}) \exp\left(-\int_0^{l_i} \lambda^{-1}(\tau_i + s) ds\right), \quad \lambda^{-1} = \sigma \rho$$

- Radiative and collisional energy loss per scattering

$$\Delta E_{tot,i} = \Delta E_{rad,i} + \Delta E_{col,i}$$

- Transverse momentum kick per scattering

$$\Delta k_{t,i}^2 = \left(E - \frac{t_i}{2m_{0i}}\right)^2 - \left(p - \frac{E}{p} \frac{t_i}{2m_{0i}} - \frac{t_i}{2p}\right)^2 - m_q^2$$

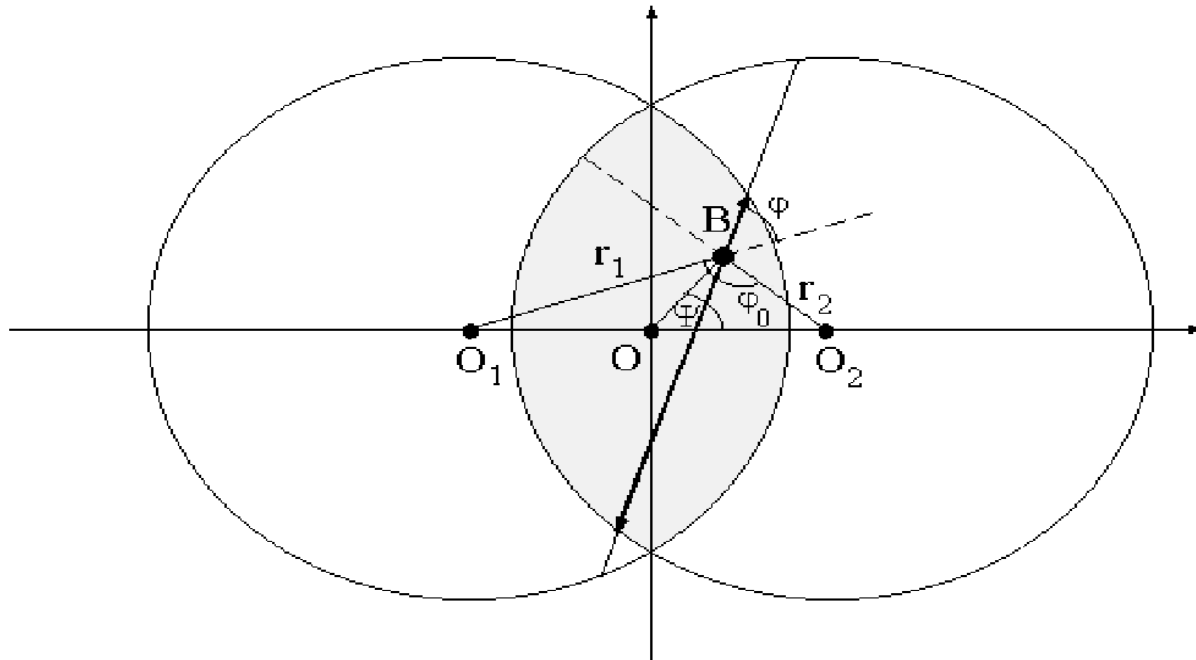
Monte-Carlo simulation of hard component (including nuclear shadowing) in HYDJET/HYDJET++

- Calculating the number of hard NN sub-collisions $N_{jet}(b, P_{tmin}, \sqrt{s})$ with $P_t > P_{tmin}$ around its mean value according to the binomial distribution.
- Selecting the type (for each of N_{jet}) of hard NN sub-collisions (pp , np or nn) depending on number of protons (Z) and neutrons ($A-Z$) in nucleus A according to the formula: $Z = A / (1.98 + 0.015A^{2/3})$.
- Generating the hard component by calling PYQUEN n_{jet} times.
- Correcting the PDF in nucleus by the accepting/rejecting procedure for each of N_{jet} hard NN sub-collisions: comparison of random number generated uniformly in the interval $[0,1]$ with shadowing factor $S(r_1, r_2, x_1, x_2, Q^2) \leq 1$ taken from the adapted impact parameter dependent parameterization based on Glauber-Gribov theory (*K. Tywoniuk et al., Phys. Lett. B 657 (2007) 170*).

Nuclear geometry and QGP evolution

impact parameter $b \equiv |O_1 O_2|$ - transverse distance between nucleus centers

$$\varepsilon(r_1, r_2) \propto T_A(r_1) * T_A(r_2) \quad (T_A(b) - \text{nuclear thickness function})$$



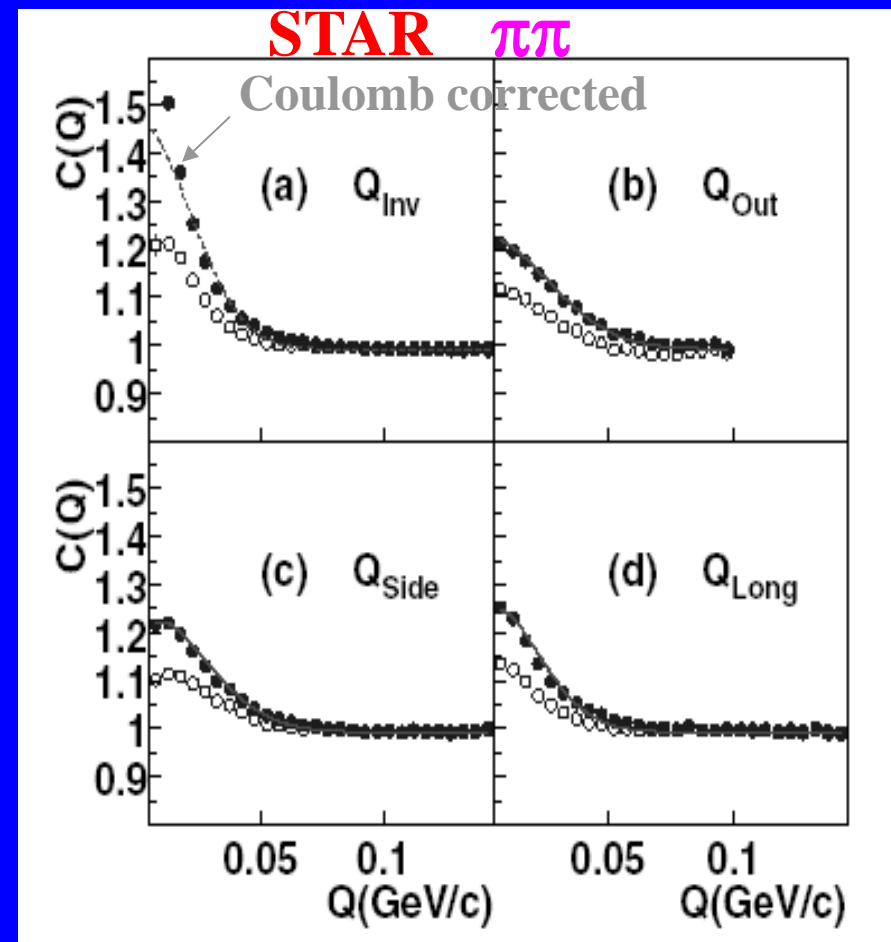
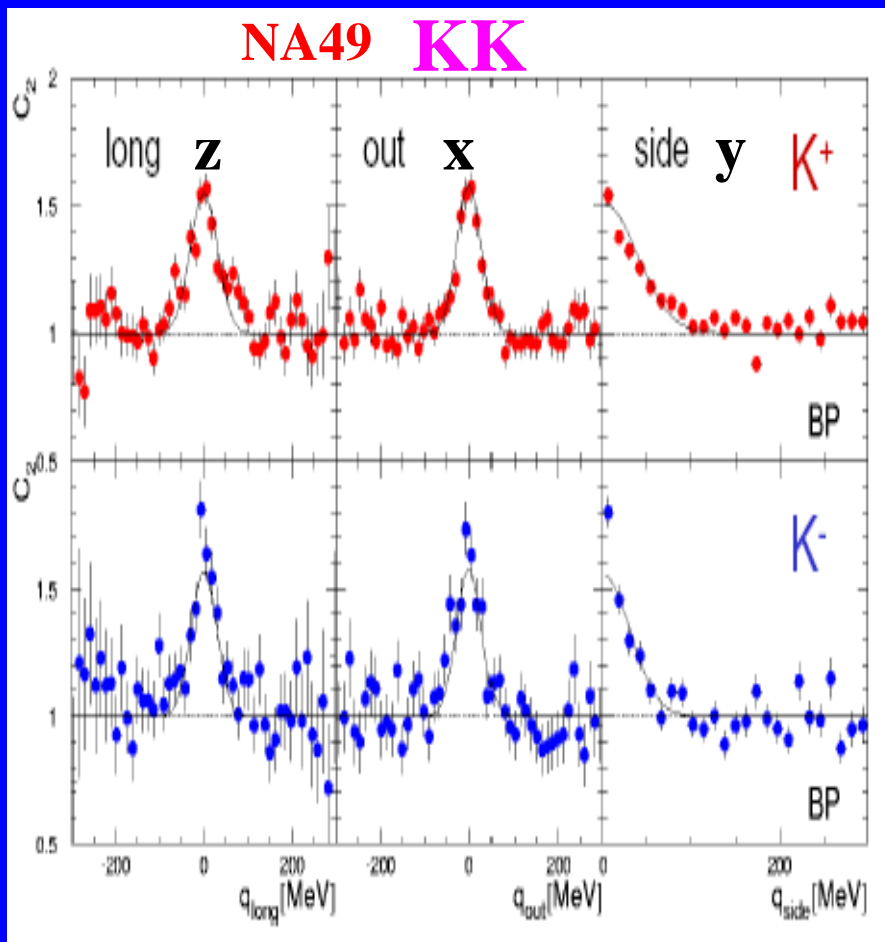
Space-time evolution of QGP, created in region of initial overlapping of colliding nuclei, is described by Lorenz-invariant Bjorken's hydrodynamics J.D. Bjorken, PRD 27 (1983)
140

3-dim fit: $CF = 1 + \lambda \exp(-R_x^2 q_x^2 - R_y^2 q_y^2 - R_z^2 q_z^2 - 2R_{xz}^2 q_x q_z)$

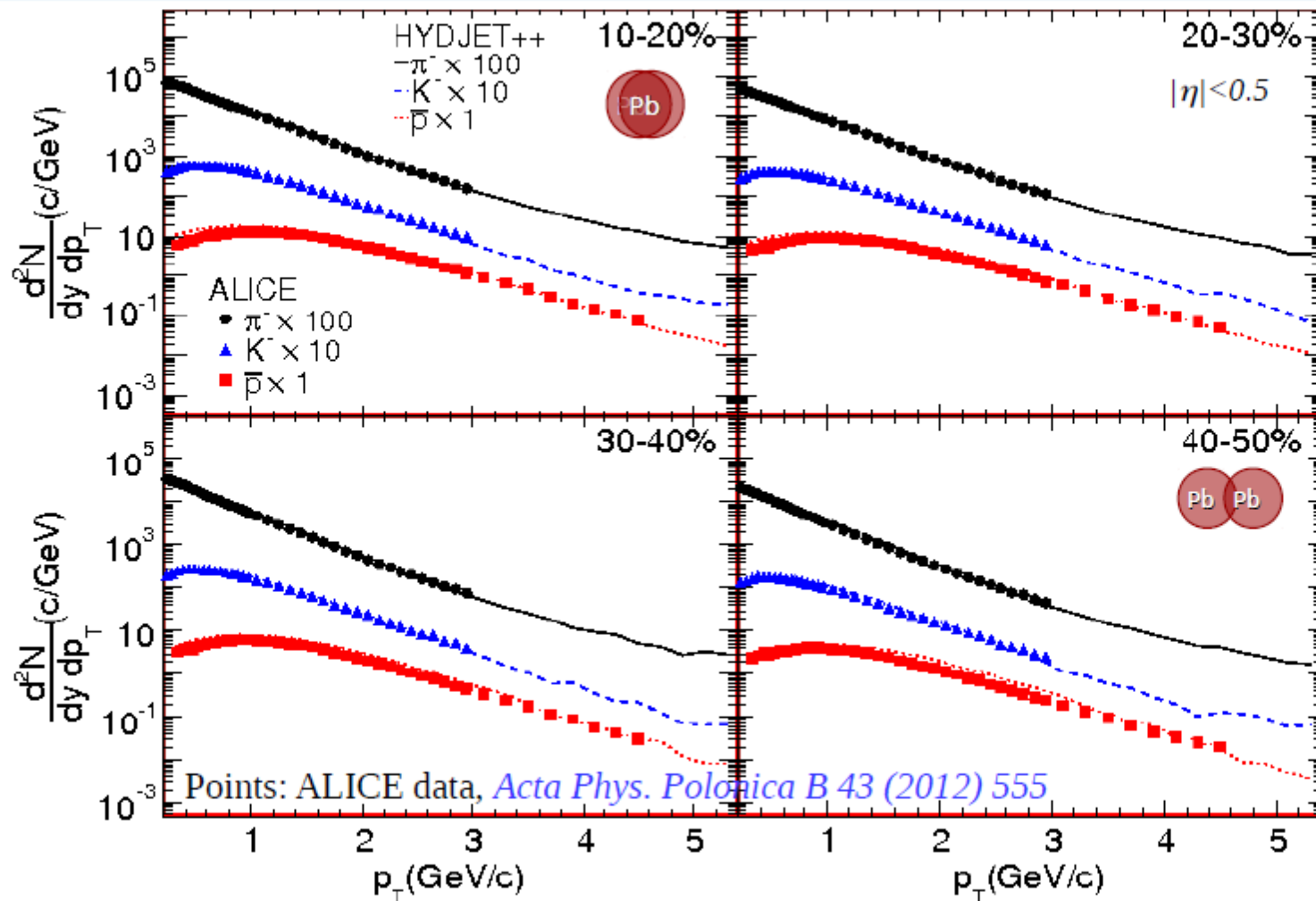
Correlation strength or chaoticity

Femtoscopy / Interferometry radii

Examples CF data: NA49 & STAR

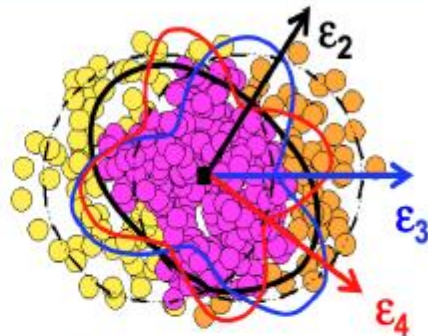
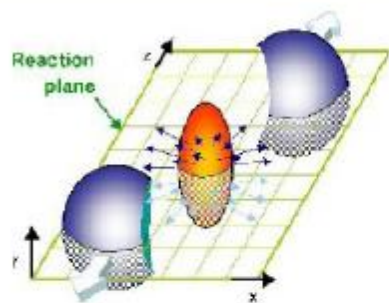


p_T -spectra of identified hadrons



HYDJET++ reproduces p_T -spectrum of pions, kaons and (anti-)protons.

Anisotropic flow in heavy ion collisions



$$E \frac{d^3N}{d^3p} = \frac{1}{\pi} \frac{d^2N}{dp_t^2 dy} \left[1 + 2 \sum_{n=1}^{\infty} v_n \cos n(\phi - \Psi_n) \right]$$

Global collective flow
w.r.t collision geometry

Eccentricity fluctuations → flow
fluctuation and odd harmonics

v_2 and v_3 in HYDJET++ are due to modification of p_T distribution coming from:
in soft part **in hard part**

- Space modulation of freeze-out surface (for v_2 and v_3)
- Velocity modulation of fireball expansion (for v_2 only)

- Energy loss path length dependence (for v_2 only)

$$R(b, \phi) = R_f(b) \frac{\sqrt{1 - \epsilon^2(b)}}{\sqrt{1 + \epsilon(b) \cos 2\phi}} [1 + \epsilon_3(b) \cos 3(\phi + \Psi_3^{\text{RP}})] \quad \Psi_3 \neq \Psi_2$$

$$\tan \varphi_{\text{sa}} = \sqrt{\frac{1 - \delta(b)}{1 + \delta(b)}} \tan \varphi.$$

φ_{u} : azimuthal angle of liquid velocity vector

φ : space azimuthal angle